On the statics and dynamics of granular-microstructured rods with higher order effects

Nima Nejadsadeghi[1] and Anil Misra[2*]

[1]Mechanical Engineering Department,
University of Kansas, 1530 W 15th Street, Learned Hall, Lawrence, KS 66047-7609
[2]Civil, Environmental and Architectural Engineering Department,
University of Kansas, 1530 W 15th Street, Learned Hall, Lawrence, KS 66045-7609.
*corresponding author: Ph: (785) 864-1750, Fax: (785) 864-5631, Email: amisra@ku.edu

For possible publication in:

Mathematics and Mechanics of Solids

Abstract

Granular-microstructured rods show strong dependence of grain-scale interactions in their mechanical behavior, and therefore, their proper description requires theories beyond the classical theory of continuum mechanics. Recently, the authors have derived a micromorphic continuum theory of degree n based upon the granular micromechanics approach (GMA). Here, the GMA is further specialized for a one-dimensional material with granular microstructure that can be described as a micromorphic medium of degree 1. To this end, the constitutive relationships, governing equations of motion and variationally consistent boundary conditions are derived. Furthermore, the static and dynamic length scales are linked to the second gradient stiffness and micro-scale mass density distribution, respectively. The behavior of a one-dimensional granular structure for different boundary conditions is studied in both static and dynamic problems. The effect of material constants and the size effects on the response of the material is also investigated through parametric studies. In the static problem, the size-dependency of the system is observed in the width of the emergent boundary layers for certain imposed boundary conditions. In the dynamic problem, microstructural effects are always present and are manifested as deviations in the natural frequencies of the system from their classical counterparts.

Keywords: free vibration; micromorphic theory; size effect; granular micromechanics; microstructured solids.

1. Introduction

Small-sized structures are being increasingly utilized in applications such as nano- and micro-electro-mechanical systems (NEMS/MEMS) and Atomic Force Microscopes (AFMs). In these structures, the effect of the microstructure on the behavior of the material is significant. Such a microstructure can be the constituent grains in a granular medium or a collection of beam elements in pantographic materials [1]. In addition, microstructured materials have also been widely used in the context of mechanical metamaterials to obtain desired unusual behavior that natural materials do not exhibit [2, 3]. For such materials (or structures depending on the scale of observation), there exists inconsistencies between the experimental findings and the classical continuum mechanics predictions [4–7]. Such variations in the observed behavior and classical continuum theory predictions pertain to the existence of the micro-mechano-morphological effects. These effects on the mechanical behavior of the materials become noticeable, especially in dynamic problems where the wavelengths of excitation are comparable to the characteristic lengths of such systems [8]. To account for the discrepancies between the theoretical predictions and experimental observations, and to overcome the inherent limitations of the classical continuum theory, non-classical continuum theories were developed, among which we refer to the works in [9–14].

To investigate the predictions of such non-classical theories, one-dimensional models are often utilized. A particular widely-studied example of such one-dimensional structures is rods. There have been several recently published articles on the analysis of one-dimensional rods utilizing non-classical continuum theories such as stress gradient (also called nonlocal), strain gradient (also called gradient elasticity), and nonlocal strain gradient models to capture the microstructural effects in static and dynamic problems [15–32]. We note that these effects have also been reported in the studies concerned with the vibration and buckling phenomena in beams, e.g. in [33–36], small-scaled truss and frame models, e.g., in [37], two-dimensional problems, e.g., in [38, 39], and metamaterials [40].

In the present paper, we expound upon a particular form of a microstructured solid, namely a one-dimensional material with granular microstructure, which is modeled as a micromorphic media of degree one using the granular micromechanics approach (GMA). GMA is a micromorphic theory equipped with an enriched kinematics to describe grain motion, in which the derived governing

equations of motion constituents are related to the granular mechano-structure of the material [41, 42]. The mathematical model derived through GMA has shown interesting results in the prediction of acoustic (material deformation) and optical (internal deformation) wave branches in granular media undergoing excitation [43–45]. The dispersive behavior predicted by GMA reflects many aspects of granular structures dynamic behavior (e.g., existence of frequency band gaps and negative group velocity), and can potentially be employed to obtain the continuum material constants of granular media [46–48].

It is notable that the dispersion analysis of infinite media does not fully reveal the effects of the length scale parameters and the applied boundary conditions on the behavior of the granular media. Therefore, it is our purpose here to further elucidate the contribution of different length scale parameters, stiffness and inertial measures (micro-mechano-morphology) to the behavior of finite length one-dimensional granular media in both static and dynamic uniaxial loading under different boundary conditions. Such analyses are essential for understanding the complex behavior of such media and to help designing suitable experimental setup to extract and identify the material parameters defining granular materials, which currently proves challenging, if not impossible. Moreover, the findings of the present paper help analyzing a myriad of granular materials found in nature, as well as serve as a design tool to conceive granular metamaterials that can be realized through additive manufacturing technologies for particular applications [49, 50].

The structure of the paper is as follows. Section 2 describes the granular micromechanics approach to model one-dimensional continua with granular microstructure. Section 3 is devoted to the static behavior analysis of one-dimensional continua with granular microstructure subjected to different boundary conditions. In section 4, the dynamic behavior of one-dimensional continua with granular microstructure is investigated through free vibration analysis. Finally, section 5 presents the summary of the work and the concluding remarks.

2. GMA based micromorphic theory of degree 1 for a 1D rod

This section introduces the continuum framework for GMA based micromorphic theory of degree 1 to model a one-dimensional granular structure. The model adopted in the current paper assumes linear elastic mechanisms of deformation with no damping. The references [41, 42, 45] describe

the framework for a three-dimensional granular structure. The reader is referred to the mentioned articles for more detailed description.

2.1.Kinematic variables

Let us consider a one-dimensional object of length L with an underlying granular microstructure composed of many grains with random mechanical and inertial properties (hereafter referred as 1D granular rod), as shown in Fig. 1. At the spatial scale, in which the object may be treated as a continuum, the material point P can be identified using the macro-scale coordinate system X. Material point P is considered to have the macro-scale linear mass density ρ (given as mass per unit length), differential length dX, and differential mass of $dm = \rho dX$ in the initial configuration. We denote by X and $x = \Xi(X,t)$ the position of the point P at initial and current configurations, respectively, where Ξ is the macro-scale placement function and t denotes time. The macro-scale displacement is defined as $u = x - X$. At a finer spatial scale, material point P is a collection of grains and is referred to as a volume element (VE) with length $L' = dX$. For a periodic granular structure, such as a granular composite made of several grains repeating periodically, the VE is identical to the notion of a unit cell, and for non-periodic granular structures, it is the volume of the granular material over which the local (micro-scale) deformation is homogenized. In the latter case, the VE is chosen as per the requirement of the mechanical problem and such that it contains sufficiently large number of grains to justify the continuity assumption. The position of each grain within the VE is identified using the micro-scale coordinate system X' of the finer spatial scale. This coordinate system is attached to the center of mass (COM) of the material point P, is taken to be parallel to the macro-scale coordinate system X, and displaces in consonance with the macro-scale displacement u. The micro-scale displacement u' is expressed as $u' = x' - X'$ where X' and $x' = \Xi'(X,X',t)$ denote the position vectors of a grain centroid at initial and current configurations, respectively, and Ξ' is the micro-scale placement function. We assume that both the micro- and macro-scale deformations are infinitesimal, and are continuous and differentiable functions of the micro- and macro-scale coordinates up to the desired order, such that we can write

$$u = u(x,t), \quad u' = u'(x,x',t). \tag{1}$$

For a micromorphic theory of degree 1, the micro-scale displacement *u'* can be written in the form below using a polynomial expansion with respect to *x'* about the COM of the VE [41].

$$u' = \psi_{11} x' + \psi_{111} \left(x' \right)^2 . \tag{2}$$

In Eq. (2), ψ_{11} and ψ_{111} are functions of *x* and *t* only, and account for the local deformation within the VE. We note that although for systems with small number of particles (or layers in composites modeled as one dimensional) a more accurate approximation of displacement can be made by subdividing the VE into different regions with different strain regimes (e.g., see [51, 52]), for large number of particles (or layers), such approaches become increasingly complicated and a linear or quadratic approximation within the whole domain of VE remains the most feasible (e.g., see [53]). We note here that efforts at formal homogenization (continualization) of mass-spring systems, such as in [54, 55], also propose multiscale decomposition of displacement field among the possible approaches for developing continuum models. Using Eq. (2), the total displacement vector for the grains within the VE are written as

$$\phi = u + u' = \bar{\phi} + \psi_{11} x' + \psi_{111} \left(x' \right)^2 . \tag{3}$$

where $\bar{\phi} = u$ is adopted such that the variable names are in harmony with previous publications [41, 42]. For a micromorphic theory of degree one, we utilize the following relative deformation measures [12, 13, 41]

$$\gamma_{11} = \bar{\phi}_{,x} - \psi_{11}, \quad \gamma_{111} = \psi_{11,x} - \psi_{111}, \tag{4}$$

where, hereafter, differentiation with respect to the spatial coordinates is denoted by a comma in the subscript. In Eq. (4), the differentiation is performed with respect to the macro-scale coordinate system. For a micromorphic theory of degree 1, and as a constitutive choice, we assume here that the relative deformation measure γ_{111} vanishes, therefore we have $\psi_{111} = \psi_{11,x}$. Note that if we further assume that the relative deformation measure γ_{11} vanishes, a second gradient model is obtained [41].

The relative displacement between two neighboring grains n and p, δ^{np}, can be written, using Eq. (3) and Eq. (4), as

$$\delta^{\mathrm{np}} = \phi^{\mathrm{p}} - \phi^{\mathrm{n}} = \delta^{\mathrm{M}} - \delta^{\mathrm{m}} + \delta^{\mathrm{g}}, \tag{5}$$

where the following micro-scale kinematic measures are introduced

$$\delta^{\mathrm{M}} = \bar{\phi}_{,x} J_1^{\mathrm{np}}, \quad \delta^{\mathrm{m}} = \gamma_{11} J_1^{\mathrm{np}}, \quad \delta^{g} = \psi_{11,x} J_2^{\mathrm{np}}. \tag{6}$$

In Eq. (6), δ^{M} signifies the portion of the relative displacement due to the macro-scale displacement gradient $\bar{\phi}_{,x}$, δ^{m} represents the portion of the relative displacement due to the fluctuation between the macro-scale displacement gradient $\bar{\phi}_{,x}$ and the micro-scale kinematic measure ψ_{11}, and δ^{g} denotes the portion of the relative displacement due to the second gradient term. Furthermore, we have defined the geometry moment measures $J_1^{\mathrm{np}} = l^{\mathrm{p}} - l^{\mathrm{n}}$ and $J_2^{\mathrm{np}} = l^{\mathrm{p}} l^{\mathrm{p}} - l^{\mathrm{n}} l^{\mathrm{n}}$, where l^{q} represents the vector joining the COM of the RVE to the grain q centroid. Note that $J_2^{\mathrm{np}} = \left(l^{\mathrm{p}} - l^{\mathrm{n}}\right)\left(l^{\mathrm{p}} + l^{\mathrm{n}}\right) = J_1^{\mathrm{np}}\left(l^{\mathrm{p}} + l^{\mathrm{n}}\right)$ which implies that for grains *n* and *p*, the farther they are from the COM of the VE, the higher the second gradient contribution to the relative displacement, δ^{g}.

2.2. Constitutive equations

We assume the macro-scale deformation energy density to be a function of the continuum kinematic measures $\bar{\phi}_{,x}$, γ_{11}, and $\psi_{11,x}$, i.e., of the form $W = W(\bar{\phi}_{,x}, \gamma_{11}, \psi_{11,x})$. Macro-scale stress measures, namely, Cauchy stress, τ_{11}, relative stress, σ_{11}, and double stress, μ_{111}, are defined as conjugates to the continuum kinematic measures, and expressed as

$$\tau_{11} = \frac{\partial W}{\partial \bar{\phi}_{,x}}, \quad \sigma_{11} = \frac{\partial W}{\partial \gamma_{11}}, \quad \mu_{111} = \frac{\partial W}{\partial \psi_{11,x}}. \tag{7}$$

The macro-scale deformation energy density can also be expressed in terms of the micro-scale deformation energy density as

$$W = \frac{1}{L'} \sum_{\alpha} W^{\alpha}\left(\delta^{\alpha \mathrm{M}}, \delta^{\alpha \mathrm{m}}, \delta^{\alpha \mathrm{g}}\right), \tag{8}$$

where W^{α} represents the micro-scale deformation energy for the α^{th} interacting pair of grains within the VE. Intergranular forces can be defined as conjugates to the micro-scale kinematic measures as

$$\frac{\partial W^{\alpha}}{\partial \delta^{\alpha M}} = f^{\alpha M}, \quad \frac{\partial W^{\alpha}}{\partial \delta^{\alpha m}} = f^{\alpha m}, \quad \frac{\partial W^{\alpha}}{\partial \delta^{\alpha g}} = f^{\alpha g}. \tag{9}$$

Substituting Eq. (8) in Eq. (7) and employing Eq. (6) and Eq. (9), the macro-scale stress measures are expressed as

$$\tau_{11} = \frac{1}{L'}\sum_{\alpha} f^{\alpha M} J_1^{\alpha}, \quad \sigma_{11} = \frac{1}{L'}\sum_{\alpha} f^{\alpha m} J_1^{\alpha}, \quad \mu_{111} = \frac{1}{L'}\sum_{\alpha} f^{\alpha g} J_2^{\alpha}. \tag{10}$$

Eq. (10) defines the macro-scale stress measures in terms of micro-scale force measures and geometry moment measures, where J_1^{α} and J_2^{α} for the α^{th} grain pair for interacting grains n and p are evaluated as J_1^{np} and J_2^{np}, respectively.

For formulating micro-scale constitutive equations relating micro-scale kinematic measures to their conjugate intergranular force measures, the following form for the micro-scale deformation energy for the α^{th} grain pair is considered

$$W^{\alpha} = \frac{1}{2}K^{\alpha M}\left(\delta^{\alpha M}\right)^2 + \frac{1}{2}K^{\alpha m}\left(\delta^{\alpha m}\right)^2 + K^{\alpha Mm}\delta^{\alpha M}\delta^{\alpha m} + \frac{1}{2}K^{\alpha g}\left(\delta^{\alpha g}\right)^2. \tag{11}$$

Based on Eq. (11), there are four linear mechanisms involved in the deformation of a grain pair in contact, each quadratic in form. $K^{\alpha i}, i = \mathrm{M,m,Mm,g}$ are the stiffnesses associated with their corresponding mechanisms.

Intergranular forces introduced in Eq. (9) are obtained, using Eq. (11), as

$$\begin{aligned} f^{\alpha M} &= \frac{\partial W^{\alpha}}{\partial \delta^{\alpha M}} = K^{\alpha M}\delta^{\alpha M} + K^{\alpha Mm}\delta^{\alpha m}, \\ f^{\alpha m} &= \frac{\partial W^{\alpha}}{\partial \delta^{\alpha m}} = K^{\alpha m}\delta^{\alpha m} + K^{\alpha Mm}\delta^{\alpha M}, \\ f^{\alpha g} &= \frac{\partial W^{\alpha}}{\partial \delta^{\alpha g}} = K^{\alpha g}\delta^{\alpha g}. \end{aligned} \tag{12}$$

Finally, using Eq. (12), the macro-scale constitutive relationships in Eq. (10) are described as

$$\tau_{11} = \left(C^{\mathrm{M}} + C^{\mathrm{Mm}}\right)\bar{\phi}_{,x} - C^{\mathrm{Mm}}\psi_{11},$$
$$\sigma_{11} = \left(C^{\mathrm{Mm}} + C^{\mathrm{m}}\right)\bar{\phi}_{,x} - C^{\mathrm{m}}\psi_{11}, \tag{13}$$
$$\mu_{111} = C^{\mathrm{g}}\psi_{11,x},$$

where the macro-scale stiffnesses C^{M}, C^{m}, C^{Mm}, and C^{g} are expressed as

$$C^{\mathrm{M}} = \frac{1}{L'}\sum_{\alpha} K^{\alpha\mathrm{M}} J_1^{\alpha} J_1^{\alpha}, \quad C^{\mathrm{m}} = \frac{1}{L'}\sum_{\alpha} K^{\alpha\mathrm{m}} J_1^{\alpha} J_1^{\alpha},$$
$$C^{\mathrm{Mm}} = \frac{1}{L'}\sum_{\alpha} K^{\alpha\mathrm{Mm}} J_1^{\alpha} J_1^{\alpha}, \quad C^{\mathrm{g}} = \frac{1}{L'}\sum_{\alpha} K^{\alpha g} J_2^{\alpha} J_2^{\alpha}. \tag{14}$$

For the stiffnesses introduced in Eq. (14), the superscript M denotes the stiffness due to macro-scale deformation, the superscript m denotes the micro-scale (relative deformation) stiffness that acts analogous to the shear rigidity in Timoshenko beam model, the superscript Mm denotes the coupling (cross-linking) stiffness between the macro- and micro-scale deformations, and the superscript g denotes the second gradient stiffness. We note here that the stiffness measures in Eq. (14) possess inherent length scales within their definitions that are natural consequences of the assumed kinematic field of motion for the grains. Accordingly, $\sqrt{\frac{C^{\mathrm{g}}}{C^{\mathrm{M}}}}$ is considered as the static length scale for the current problem.

2.3. Governing equations of motion

Hamilton's principle is used to obtain equations of motion for the 1D granular rod. Hamilton's principle requires the action functional to be minimum, and is expressed as

$$\int_{t_0}^{t_1}\left(\delta\breve{T} - \delta\breve{W} + \delta\breve{W}_{ext}\right)dt = 0, \tag{15}$$

where δ is the variation symbol and the terms $\breve{T}$, $\breve{W}$, and $\breve{W}_{ext}$ are defined in the following. The term $\breve{T} = \int_L T dx$ is the total kinetic energy of the granular structure, in which T is the kinetic energy density, utilizing König's theorem [56] defined and expanded as [41]

$$T = \frac{1}{L'}\int_{L'}\frac{1}{2}\rho'\dot{\phi}\dot{\phi}dx' = \frac{1}{2}\rho\dot{\bar{\phi}}\dot{\bar{\phi}} + \frac{1}{2}\rho_{11}\dot{\psi}_{11}\dot{\psi}_{11} + \rho_{111}\dot{\psi}_{11}\dot{\psi}_{11,x} + \frac{1}{2}\rho_{1111}\dot{\psi}_{11,x}\dot{\psi}_{11,x}. \tag{16}$$

In Eq. (16), ρ' is the micro-scale mass density per unit macro-volume, and over-dots here and henceforward represent differentiation with respect to time. The following inertia measures have been defined [41]

$$\rho=\frac{1}{L'}\int_{L'}\rho' dx',\quad \rho_{11}=\frac{1}{L'}\int_{L'}\rho'\left(x'\right)^2 dx',\quad \rho_{111}=\frac{1}{L'}\int_{L'}\rho'\left(x'\right)^3 dx',\quad \rho_{1111}=\frac{1}{L'}\int_{L'}\rho'\left(x'\right)^4 dx' \text{ .(17)}$$

The term ρ represents the macro-scale mass density and is an average of the micro-scale mass density ρ' within the VE. On the other hand, the other inertia measures introduced in Eq. (17) are functions of the micro-scale mass density and its spatial distribution and inherently include the length scales existing in the dynamic problem. In particular, the inertia measure ρ_{111} is due to non-symmetric micro-scale mass density distribution in the VE, e.g., for a graded granular material in micro-scale, and vanishes for symmetric micro-scale mass density distributions [45]. Interestingly, and as a consequence of Eq. (17), these length scales are not independent, but are related to each other through the micro-scale mass density ρ' distribution. In other words, for a known micro-scale mass density ρ' distribution within the VE, these length scales are fixed [45]. The kinetic energy introduced in Eq. (16) results from the assumed kinematic field in Eq. (3). We note that the additional velocity gradient terms appearing in Eq. (16) are not postulated *a priori* as often done in higher order continuum modeling (which are typically introduced to improve the dispersion predictions). This form of kinetic energy includes terms that are absent in classical continuum mechanics formulation to account for the non-uniform distribution of velocity in the VE, and expands upon the terms currently postulated in nonlocal strain gradient elasticity (e.g. in [31]). The existence of velocity gradient terms in the description of the kinetic energy has also been observed in gradient elasticity models to describe lattices with distributed mass properties [15] and in works concerning modeling the effect of micro-inertia in heterogeneous materials, e.g., in [57]. Moreover, velocity gradient terms have been also adopted to model wave dispersion in nonlinear pantographic beams and related to the distributed masses along the rigid links [58]. For the kinetic energy in Eq. (16) to be positive definite, the inequality $\rho_{11}\rho_{1111}-\rho_{111}^2>0$ must hold. This inequality is obtained by rewriting Eq. (16) in the form $T=\frac{1}{2}\breve{\mathbf{x}}^{\mathrm{T}}\breve{\mathbf{A}}\breve{\mathbf{x}}$, where $\breve{\mathbf{x}}=\left[\dot{\phi}\ \dot{\psi}_{11}\ \dot{\psi}_{11,x}\right]^{\mathrm{T}}$, and requiring that the matrix $\breve{\mathbf{A}}$ be positive definite.

In Eq. (15), $\delta\breve{W} = \int_L \delta W dx$ represents the variation of total macro-scale deformation energy, expressed as

$$\delta\breve{W} = -\int_L \left(\tau_{11} + \sigma_{11}\right)_{,x} \delta\bar{\phi}\, dx - \int_L \left(\mu_{111,x} + \sigma_{11}\right)\delta\psi_{11} dx + \left(\tau_{11} + \sigma_{11}\right)\delta\bar{\phi}\Big|_{x=0}^{x=L} + \mu_{111}\delta\psi_{11}\Big|_{x=0}^{x=L}. \tag{18}$$

Finally, the term $\delta\breve{W}_{ext}$ in Eq. (15) corresponds to the variation of total external energy defined as

$$\delta\breve{W}_{ext} = \int_L \underline{f}\,\delta\bar{\phi}\, dx + \int_L \underline{\Phi}\,\delta\psi_{11} dx + \underline{t}\,\delta\bar{\phi}\Big|_{x=0}^{x=L} + \underline{T}\,\delta\psi_{11}\Big|_{x=0}^{x=L}. \tag{19}$$

In Eq. (19), $\underline{f}$ is the non-contact body force per unit length, $\underline{t}$ is the contact traction, $\underline{\Phi}$ is the non-contact body double force per unit length, and $\underline{T}$ is the contact double traction. Substituting Eq. (16), Eq. (18), and Eq. (19) in the expression for Hamilton's principle in Eq. (15) results in

$$\begin{aligned}
&\int_{t_0}^{t_1}\int_L \left[\left(\tau_{11} + \sigma_{11}\right)_{,x} + \underline{f} - \rho\ddot{\bar{\phi}}\right]\delta\bar{\phi}\, dx dt \\
&+\int_{t_0}^{t_1}\int_L \left[\sigma_{11} + \mu_{111,x} + \underline{\Phi} - \rho_{11}\ddot{\psi}_{11} + \rho_{1111}\ddot{\psi}_{11,xx} + \left(\rho_{111}\right)_{,x}\ddot{\psi}_{11} + \left(\rho_{1111}\right)_{,x}\ddot{\psi}_{11,x}\right]\delta\psi_{11} dx dt \\
&+\int_{t_0}^{t_1}\left[\left(\underline{t} - \tau_{11} - \sigma_{11}\right)\delta\bar{\phi}\right]_{x=0}^{x=L} dt + \int_{t_0}^{t_1}\left[\left(\underline{T} - \rho_{111}\ddot{\psi}_{11} - \rho_{1111}\ddot{\psi}_{11,x} - \mu_{111}\right)\delta\psi_{11}\right]_{x=0}^{x=L} dt = 0
\end{aligned} \tag{20}$$

From Eq. (20) it follows that, after assuming zero non-contact body forces and double forces, using the constitutive equations in Eq. (13), and assuming spatial independence of the macro-scale stiffnesses, the equations of motion for the problem domain $0 \le x \le L$ are expressed as

$$\left(C^{\mathrm{M}} + C^{\mathrm{m}} + 2C^{\mathrm{Mm}}\right)\bar{\phi}_{,xx} - \left(C^{\mathrm{m}} + C^{\mathrm{Mm}}\right)\psi_{11,x} = \rho\ddot{\bar{\phi}}\,, \tag{21a}$$

$$C^{\mathrm{g}}\psi_{11,xx} + \left(C^{\mathrm{Mm}} + C^{\mathrm{m}}\right)\bar{\phi}_{,x} - C^{\mathrm{m}}\psi_{11} = \rho_{11}\ddot{\psi}_{11} - \rho_{1111}\ddot{\psi}_{11,xx} - \left(\rho_{111}\right)_{,x}\ddot{\psi}_{11} - \left(\rho_{1111}\right)_{,x}\ddot{\psi}_{11,x}. \tag{21b}$$

From Eq. (20), the boundary conditions are stated as

$$\left(\underline{t} - \left(C^{\mathrm{M}} + C^{\mathrm{m}} + 2C^{\mathrm{Mm}}\right)\bar{\phi}_{,x} + \left(C^{\mathrm{m}} + C^{\mathrm{Mm}}\right)\psi_{11}\right)\delta\bar{\phi} = 0 \quad \text{at } x = 0 \text{ and } L\,, \tag{22a}$$

$$\left(\underline{T} - \rho_{111}\ddot{\psi}_{11} - \rho_{1111}\ddot{\psi}_{11,x} - C^{\mathrm{g}}\psi_{11,x}\right)\delta\psi_{11} = 0 \quad \text{at } x = 0 \text{ and } L\,. \tag{22b}$$

We remark the presence of terms with time derivative in the boundary conditions in Eq. (22b). The existence of time derivative terms in the boundary conditions are also discussed in the analysis of nonlocal strain gradient rods [31].

In this paper, we assume that the micro-scale mass density, ρ', is constant in both micro- and macro-scale coordinate systems. Consequently, the equations of motion reduce to

$$\left(C^{\mathrm{M}}+C^{\mathrm{m}}+2C^{\mathrm{Mm}}\right)\bar{\phi}_{,xx}-\left(C^{\mathrm{m}}+C^{\mathrm{Mm}}\right)\psi_{11,x}=\rho\ddot{\bar{\phi}}\,, \tag{23a}$$

$$C^{\mathrm{g}}\psi_{11,xx}+\left(C^{\mathrm{Mm}}+C^{\mathrm{m}}\right)\bar{\phi}_{,x}-C^{\mathrm{m}}\psi_{11}=\rho_{11}\ddot{\psi}_{11}-\rho_{1111}\ddot{\psi}_{11,xx}\,. \tag{23b}$$

Moreover, the boundary conditions in Eq. (22) reduce to

$$\left(\underline{t}-\left(C^{\mathrm{M}}+C^{\mathrm{m}}+2C^{\mathrm{Mm}}\right)\bar{\phi}_{,x}+\left(C^{\mathrm{m}}+C^{\mathrm{Mm}}\right)\psi_{11}\right)\delta\bar{\phi}=0 \quad \text{at } x=0 \text{ and } L\,, \tag{24a}$$

$$\left(\underline{T}-\rho_{1111}\ddot{\psi}_{11,x}-C^{\mathrm{g}}\psi_{11,x}\right)\delta\psi_{11}=0 \quad \text{at } x=0 \text{ and } L\,. \tag{24b}$$

2.4. Dimensionless form of the governing equations

For further discussion, it is useful to reduce the number of parameters by nondimensionalizing the equations of motion in Eq. (23) to exclude the explicit physical parameters of the system. To this end, we first define three dynamic length scales l_1, l_2, and l_3 as

$$l_1^2=\frac{\rho_{11}}{\rho},\quad l_2^3=\frac{\rho_{111}}{\rho},\quad l_3^4=\frac{\rho_{1111}}{\rho}\,, \tag{25}$$

which, for the constant micro-scale mass density, ρ', lead to $l_1^2=\dfrac{(L')^2}{12}$, $l_2^3=0$, $l_3^4=\dfrac{(L')^4}{80}$, where *L'* is the VE size [45]. Additionally, we introduce the following dimensionless variables and parameters

$$\tilde{\bar{\phi}}=\frac{\bar{\phi}}{L},\quad \tilde{\psi}_{11}=\psi_{11},\quad \tilde{x}=\frac{x}{L},\quad \tilde{t}=\frac{t}{\sqrt{\dfrac{\rho L^2}{C^{\mathrm{M}}}}},\quad \alpha_m=\frac{C^{\mathrm{m}}}{C^{\mathrm{M}}},\quad \alpha_{Mm}=\frac{C^{\mathrm{Mm}}}{C^{\mathrm{M}}},\quad l_s=\frac{1}{L}\sqrt{\frac{C^{\mathrm{g}}}{C^{\mathrm{M}}}},\quad n=\frac{L}{L'}\,. \tag{26}$$

It is understood that the parameter α_m gives the ratio of the micro-scale (relative deformation) stiffness to the macro-scale stiffness, α_{Mm} represents the ratio of the cross-linking stiffness to the macro-scale stiffness, and l_s is the dimensionless static length scale, where it is clear that larger values for l_s signify more noticeable second gradient effects. Moreover, *n* shows how large the macro-scale structure length is compared to the VE length. Now, using Eq. (25) and Eq. (26), the dimensionless form of the equations of motion in Eq. (23) is stated as

$$\left(1+\alpha_m+2\alpha_{Mm}\right)\tilde{\bar{\phi}}_{,\tilde{x}\tilde{x}}-\left(\alpha_m+\alpha_{Mm}\right)\tilde{\psi}_{11,\tilde{x}}=\ddot{\tilde{\bar{\phi}}}\,, \tag{27a}$$

$$l_s^2\tilde{\psi}_{11,\tilde{x}\tilde{x}}+\left(\alpha_m+\alpha_{Mm}\right)\tilde{\bar{\phi}}_{,\tilde{x}}-\alpha_m\tilde{\psi}_{11}=\frac{1}{12n^2}\ddot{\tilde{\psi}}_{11}-\frac{1}{80n^4}\ddot{\tilde{\psi}}_{11,\tilde{x}\tilde{x}}\,. \tag{27b}$$

The dimensionless spatial domain of the problem is $0\le\tilde{x}\le 1$. We emphasize that the coefficients on the right hand side of Eq. (27b) are not arbitrary, but are natural consequences of the assumed micro-scale mass density, ρ', distribution. Indeed, these coefficients differ if one considers a different distribution for the micro-scale mass density, ρ', within the VE [45]. We note that the dimensionless material constants α_m and α_{Mm} must satisfy the positive definiteness of the macro-scale deformation energy density. This necessitates the inequality $\alpha_m-\alpha_{Mm}^2>0$ to hold.

The dimensionless form of the boundary conditions in Eq. (24) is expressed as

$$\left(\tilde{\underline{t}}-\left(1+\alpha_m+2\alpha_{Mm}\right)\tilde{\bar{\phi}}_{,\tilde{x}}+\left(\alpha_m+\alpha_{Mm}\right)\tilde{\psi}_{11}\right)\delta\tilde{\bar{\phi}}=0 \quad \text{at } \tilde{x}=0 \text{ and } 1\,, \tag{28a}$$

$$\left(\tilde{\underline{T}}-\frac{1}{80n^4}\ddot{\tilde{\psi}}_{11,\tilde{x}}-l_s^2\tilde{\psi}_{11,\tilde{x}}\right)\delta\tilde{\psi}_{11}=0 \quad \text{at } \tilde{x}=0 \text{ and } 1\,. \tag{28b}$$

where $\tilde{\underline{t}}=\frac{\underline{t}}{C^{\mathrm{M}}}$ and $\tilde{\underline{T}}=\frac{\underline{T}}{C^{\mathrm{M}}L}$ are dimensionless contact traction and contact double traction, respectively.

The governing equations of motion in Eq. (27) result from the assumption of the existence of the relative deformation field γ_{11}, i.e., the macro-scale displacement gradient $\bar{\phi}_{,x}$ is different from the micro-scale kinematic measure ψ_{11}. They are also predicated on the assumption of the existence

of a VE with a finite size, yet very small, compared to the macroscopic length of the structure. For the case of vanishing coupling stiffness α_{Mm}, if we also assume that $\alpha_m \to \infty$, or equivalently, if the relative deformation measure γ_{11} is zero, i.e., $\tilde{\psi}_{11} = \tilde{\tilde{\phi}}_{,x}$, we obtain the governing equation of motion of the form $\left(1 - \frac{1}{12n^2}\frac{\partial^2}{\partial \tilde{x}^2} + \frac{1}{80n^4}\frac{\partial^4}{\partial \tilde{x}^4}\right)\ddot{\tilde{\tilde{\phi}}} = \left(1 - l_s^2 \frac{\partial^2}{\partial \tilde{x}^2}\right)\tilde{\tilde{\phi}}_{,\tilde{x}\tilde{x}}$. The derived equation has a more general form although it has similarities with the nonlocal strain gradient models presented in [27, 31] and the model presented in [59], where the term $\frac{1}{\sqrt{12}n}$ can be considered to be the dimensionless typical nonlocal parameter, and the term $\frac{1}{\sqrt{80}n^2}$ is considered as an additional higher gradient nonlocal parameter. Note that the model presented in [31] can be deemed as a special case of the present model with only one term as the nonlocal parameter, and the model in [59] treats the dynamic length scales as independent constants without an explicit relation to the micro-scale mass density distribution. If we further assume $\frac{L'}{L} \to 0$ (equivalently, if $n \to \infty$), we recover the equation of motion of a rod based on strain-gradient elasticity of the dimensionless form $\ddot{\tilde{\tilde{\phi}}} = \left(1 - l_s^2 \frac{\partial^2}{\partial \tilde{x}^2}\right)\tilde{\tilde{\phi}}_{,\tilde{x}\tilde{x}}$, similar to the form reported in [30]. This approximation, in the limit as $n \to \infty$, shows that for practical cases, with finite *n*, the small scale effects described by the vanishing terms cannot be assumed to be insignificant although they may not be easily detectable in large-scale structures. Finally, in the absence of the static length scale l_s, the classical form of the governing equation is retrieved.

3. Static behavior

3.1. General solution

Here we focus on the static deformation of the 1D granular rod. The governing equations in Eq. (27) for the static case reduce to the following balance equations

$$\left(1 + \alpha_m + 2\alpha_{Mm}\right)\tilde{\tilde{\phi}}_{,\tilde{x}\tilde{x}} - \left(\alpha_m + \alpha_{Mm}\right)\tilde{\psi}_{11,\tilde{x}} = 0, \tag{29a}$$

$$l_s^2\tilde{\psi}_{11,\tilde{x}\tilde{x}}+\left(\alpha_m+\alpha_{Mm}\right)\tilde{\tilde{\phi}}_{,\tilde{x}}-\alpha_m\tilde{\psi}_{11}=0\,, \tag{29b}$$

where the spatial domain for the problem is $0\le\tilde{x}\le 1$. Using Eq. (28), the boundary conditions for the static case are written as

$$\left(\underline{\tilde{t}}-\left(1+\alpha_m+2\alpha_{Mm}\right)\tilde{\tilde{\phi}}_{,\tilde{x}}+\left(\alpha_m+\alpha_{Mm}\right)\tilde{\psi}_{11}\right)\delta\tilde{\tilde{\phi}}=0 \quad \text{at } \tilde{x}=0 \text{ and } 1\,, \tag{30a}$$

$$\left(\underline{\tilde{T}}-l_s^2\tilde{\psi}_{11,\tilde{x}}\right)\delta\tilde{\psi}_{11}=0 \quad \text{at } \tilde{x}=0 \text{ and } 1. \tag{30b}$$

Here, an analytical solution for Eq. (29) is sought. To this end, Eq. (29b) is differentiated with respect to the spatial variable to obtain

$$l_s^2\tilde{\psi}_{11,\tilde{x}\tilde{x}\tilde{x}}+\left(\alpha_m+\alpha_{Mm}\right)\tilde{\tilde{\phi}}_{,\tilde{x}\tilde{x}}-\alpha_m\tilde{\psi}_{11,\tilde{x}}=0\,. \tag{31}$$

Substituting for $\tilde{\tilde{\phi}}_{,\tilde{x}\tilde{x}}$ from Eq. (29a) into Eq. (31) gives

$$\tilde{\psi}_{11,\tilde{x}\tilde{x}\tilde{x}}-\kappa^2\tilde{\psi}_{11,\tilde{x}}=0, \quad \kappa^2=\frac{\alpha_m-\alpha_{Mm}^2}{l_s^2\left(1+\alpha_m+2\alpha_{Mm}\right)}. \tag{32}$$

Eq. (32) can be readily solved to obtain a solution for the micro-scale kinematic measure, $\tilde{\psi}_{11}$, expressed as

$$\tilde{\psi}_{11}=\hat{C}_1\cosh\left(\kappa\tilde{x}\right)+\hat{C}_2\sinh\left(\kappa\tilde{x}\right)+\hat{C}_3\,, \tag{33}$$

where $\hat{C}_1$, $\hat{C}_2$, and $\hat{C}_3$ are constants of integration. From substituting Eq. (33) in Eq. (29a) it follows that

$$\tilde{\tilde{\phi}}=\frac{\alpha_m+\alpha_{Mm}}{\kappa\left(1+\alpha_m+2\alpha_{Mm}\right)}\hat{C}_1\sinh\left(\kappa\tilde{x}\right)+\frac{\alpha_m+\alpha_{Mm}}{\kappa\left(1+\alpha_m+2\alpha_{Mm}\right)}\hat{C}_2\cosh\left(\kappa\tilde{x}\right)+\hat{C}_5\tilde{x}+\hat{C}_4\,, \tag{34}$$

where $\hat{C}_4$ and $\hat{C}_5$ are additional constants of integration to be determined. The solution for the macro-scale displacement $\tilde{\tilde{\phi}}$ expressed in Eq. (34) bears similarities with the solution obtained following the strain gradient theory for a microbar in [30], and for the gradient-elastic bar in [25].

Substituting Eq. (33) and Eq. (34) in Eq. (29b) results in $\widehat{C}_5 = \widehat{C}_3$, thereby reducing the number of unknown constants from five to four.

We here consider three possible scenarios for the applied boundary conditions in order to explore the static behavior of the 1D granular rod. These boundary conditions are all following the conventional macro-scale displacement-control experimental setup where the macro-scale displacement is fixed at one end and prescribed at the other end. The three considered experiments are different in terms of the boundary conditions imposed on the micro-scale kinematic measure $\tilde{\psi}_{11}$ where either the value for $\tilde{\psi}_{11}$ (geometrical boundary condition) or the value for $\tilde{\psi}_{11,\tilde{x}}$ (natural boundary condition, i.e., the double traction) is prescribed at the ends (boundaries) of the structure. Such experiments, although performed computationally here, may help devise experiments to observe and extract micro-scale phenomena for materials with granular microstructure by demonstrating the level of the effect of the non-classical boundary conditions on the response of the system in a static case. For illustration of the predicted behavior, we consider a material with constants $\alpha_m = 0.5$, $\alpha_{Mm} = -0.4$, and $l_s = 0.05$, for all three scenarios. This choice of parameters is known to yield interesting dynamic behavior of granular structures, namely the emergence of frequency band gaps and negative group velocity, while the deformation energy remains positive definite [43, 45]. In addition, certain micro-morphologies (e.g., see structure C in [60]) yield elastic constants of similar type.

3.2. Scenario 1

In the first scenario, demonstrated in Fig. 2(a), we consider the geometric boundary conditions of the form

$$\tilde{\tilde{\phi}}(0) = 0, \quad \tilde{\psi}_{11}(0) = 0, \quad \tilde{\tilde{\phi}}(1) = \bar{\phi}_r, \quad \tilde{\psi}_{11}(1) = \psi_r. \tag{35}$$

Eq. (35) implies that on the left end of the domain, both kinematic measures are fixed, and on the right end, both kinematic measures have prescribed values. Imposing the boundary conditions in Eq. (35) results in the following system of linear equations from which the constants $\widehat{C}_1, \widehat{C}_2, \widehat{C}_3$, and $\widehat{C}_4$ are readily calculated

$$\begin{bmatrix} 0 & \dfrac{\alpha_m+\alpha_{Mm}}{\kappa\left(1+\alpha_m+2\alpha_{Mm}\right)} & 0 & 1 \\ 1 & 0 & 1 & 0 \\ \dfrac{\alpha_m+\alpha_{Mm}}{\kappa\left(1+\alpha_m+2\alpha_{Mm}\right)}\sinh(\kappa) & \dfrac{\alpha_m+\alpha_{Mm}}{\kappa\left(1+\alpha_m+2\alpha_{Mm}\right)}\cosh(\kappa) & 1 & 1 \\ \cosh(\kappa) & \sinh(\kappa) & 1 & 0 \end{bmatrix} \begin{Bmatrix} \widehat{C}_1 \\ \widehat{C}_2 \\ \widehat{C}_3 \\ \widehat{C}_4 \end{Bmatrix} = \begin{Bmatrix} 0 \\ 0 \\ \overline{\phi}_r \\ \psi_r \end{Bmatrix}. \tag{36}$$

Moreover, the dimensionless macro-scale deformation energy density $\tilde{W} = \dfrac{W}{C^{\mathrm{M}}}$ is calculated as

$$\tilde{W} = \frac{1}{2}\tilde{\tilde{\phi}}_{,\tilde{x}}{}^2 + \frac{1}{2}\alpha_m\left(\tilde{\tilde{\phi}}_{,\tilde{x}} - \tilde{\psi}_{11}\right)^2 + \alpha_{Mm}\tilde{\tilde{\phi}}_{,\tilde{x}}\left(\tilde{\tilde{\phi}}_{,\tilde{x}} - \tilde{\psi}_{11}\right) + \frac{1}{2}l_s^2\tilde{\psi}_{11,\tilde{x}}{}^2. \tag{37}$$

Fig. 3(a) corresponds to the case where $\overline{\phi}_r = 0.01$ and $\psi_r = 0$, Fig. 3(b) corresponds to the case where $\overline{\phi}_r = 0$ and $\psi_r = 0.01$, and Fig. 3(c) shows the results for the case where $\overline{\phi}_r = 0.01$ and $\psi_r = 0.01$. According to the results in Fig. 3(a), having the kinematic measure $\tilde{\psi}_{11}$ fixed has negligible observable contribution on the behavior of the macro-scale displacement $\tilde{\tilde{\phi}}$, however, results in larger energy stored in the boundary layers. From the results shown in Fig. 3(b) for the case of zero macro-scale displacement $\tilde{\tilde{\phi}}$ and imposed nonzero micro-scale kinematic measure $\tilde{\psi}_{11}$ at the right end, we observe that while macroscopically the length of the structure has not changed, regions undergoing compression and tension exist within the material. Also, due to the difference in values between the macro-scale displacement gradient $\tilde{\tilde{\phi}}_{,\tilde{x}}$ and micro-scale kinematic measure $\tilde{\psi}_{11}$, high deformation energy concentration is observed in the right boundary layer, while the rest of the material experiences negligible stored deformation energy. Fig. 3(c) results are the superposition of the two results in Fig. 3(a) and Fig. 3(b), which in terms of the macro-scale displacement $\tilde{\tilde{\phi}}$ shows near linear trend, and in terms of the deformation energy density reveals localization in the left end and uniform deformation energy density in the rest of the domain.

3.3. Scenario 2

In the second scenario with results given in Fig. 4, we consider the following boundary conditions

$$\tilde{\bar{\phi}}(0)=0,\quad \tilde{\psi}_{11,\tilde{x}}(0)=0,\quad \tilde{\bar{\phi}}(1)=\bar{\phi}_r,\quad \tilde{\psi}_{11,\tilde{x}}(1)=\psi'_r, \tag{38}$$

which, in addition to the macro-scale displacement boundary conditions, imposes zero double traction on the left end, and a prescribed double traction on the right end. Such boundary conditions lead to the following system of linear equations for the constants $\hat{C}_1, \hat{C}_2, \hat{C}_3$, and $\hat{C}_4$,

$$\begin{bmatrix} 0 & \dfrac{\alpha_m+\alpha_{Mm}}{\kappa\left(1+\alpha_m+2\alpha_{Mm}\right)} & 0 & 1 \\ 0 & \kappa & 0 & 0 \\ \dfrac{\alpha_m+\alpha_{Mm}}{\kappa\left(1+\alpha_m+2\alpha_{Mm}\right)}\sinh(\kappa) & \dfrac{\alpha_m+\alpha_{Mm}}{\kappa\left(1+\alpha_m+2\alpha_{Mm}\right)}\cosh(\kappa) & 1 & 1 \\ \kappa\sinh(\kappa) & \kappa\cosh(\kappa) & 0 & 0 \end{bmatrix} \begin{Bmatrix} \hat{C}_1 \\ \hat{C}_2 \\ \hat{C}_3 \\ \hat{C}_4 \end{Bmatrix} = \begin{Bmatrix} 0 \\ 0 \\ \bar{\phi}_r \\ \psi'_r \end{Bmatrix}. \tag{39}$$

Fig. 4(a) corresponds to the case where $\bar{\phi}_r = 0.01$ and $\psi'_r = 0$, Fig. 4(b) corresponds to the case where $\bar{\phi}_r = 0$ and $\psi'_r = 0.01$, and Fig. 4(c) shows the results for the case where $\bar{\phi}_r = 0.01$ and $\psi'_r = 0.01$. According to the results in Fig. 4(a), having the double traction zero at both ends results in a solution equal to a classical continuum. The macro-scale displacement $\tilde{\bar{\phi}}$ is perfectly linear and there is no contribution of energy due to the relative motion and second gradient deformation. Specifying a nonzero double traction on the right end, for which case the results are shown in Fig. 4(b), follows the same behavior as of the one in Fig. 3(b). For the superposition of the cases in Fig. 4(a) and Fig. 4(b), shown in Fig. 4(c), except for the right boundary layer, the energy content within the structure is equal to the classical case and the macro-scale displacement $\tilde{\bar{\phi}}$ follows an almost linear regime.

3.4. Scenario 3

In the third scenario with results presented in Fig. 5, we consider the mixed boundary conditions expressed as

$$\tilde{\bar{\phi}}(0)=0,\quad \tilde{\psi}_{11,\tilde{x}}(0)=0,\quad \tilde{\bar{\phi}}(1)=\bar{\phi}_r,\quad \tilde{\psi}_{11}(1)=\psi_r. \tag{40}$$

Similar to the approach taken in previous scenarios, the constants $\widehat{C}_1, \widehat{C}_2, \widehat{C}_3,$ and $\widehat{C}_4$ are obtained by solving the following system of linear equations

$$\begin{bmatrix} 0 & \dfrac{\alpha_m+\alpha_{Mm}}{\kappa\left(1+\alpha_m+2\alpha_{Mm}\right)} & 0 & 1 \\ 0 & \kappa & 0 & 0 \\ \dfrac{\alpha_m+\alpha_{Mm}}{\kappa\left(1+\alpha_m+2\alpha_{Mm}\right)}\sinh(\kappa) & \dfrac{\alpha_m+\alpha_{Mm}}{\kappa\left(1+\alpha_m+2\alpha_{Mm}\right)}\cosh(\kappa) & 1 & 1 \\ \cosh(\kappa) & \sinh(\kappa) & 1 & 0 \end{bmatrix} \begin{Bmatrix} \widehat{C}_1 \\ \widehat{C}_2 \\ \widehat{C}_3 \\ \widehat{C}_4 \end{Bmatrix} = \begin{Bmatrix} 0 \\ 0 \\ \overline{\phi}_r \\ \psi_r \end{Bmatrix}. \tag{41}$$

Fig. 5(a) corresponds to the case where $\overline{\phi}_r = 0.01$ and $\psi_r = 0$, Fig. 5(b) corresponds to the case where $\overline{\phi}_r = 0$ and $\psi_r = 0.01$, and Fig. 5(c) shows the results for the case where $\overline{\phi}_r = 0.01$ and $\psi_r = 0.01$. A fixed micro-scale kinematic measure at the right end in Fig. 5(a) results in large deformation energy stored in the right boundary layer and uniform energy density distribution in the rest of the domain. This stored energy can be attributed to the difference in value between the imposed macro-scale displacement gradient $\overline{\overline{\phi}}_{,\tilde{x}}$ and the micro-scale kinematic measure $\tilde{\psi}_{11}$ at the right end. The results in Fig. (5b) are qualitatively similar to those in Fig. 3(b) and Fig. 4(b) and follow the same discussion. Interestingly, the results in Fig. 5(c) are similar to the ones in Fig. 4(a). This case corresponds to a zero double traction at the left end and a prescribed value for the micro-scale kinematic measure $\tilde{\psi}_{11}$ equal to the macro-scale strain at the right end. In this case, similar to the one in Fig. 4(a), the macro-scale displacement $\overline{\overline{\phi}}$ is linear and the deformation energy density due to the macro-scale displacement gradient is the sole contributor to the total deformation energy density.

Based on the observations from the results in Figs. 3-5, the following conclusions can be drawn. First, imposing fixed and prescribed macro-scale displacements $\overline{\overline{\phi}}$ at left and right ends of the structure, respectively, one observes a classical-like behavior only if at each end, the contact double traction is held to be zero, or the micro-scale kinematic measure $\tilde{\psi}_{11}$ is assigned a value equal to the macro-scale displacement gradient $\overline{\overline{\phi}}_{,\tilde{x}}$ (macro-scale strain). For the cases where the macro-scale displacement gradient $\overline{\overline{\phi}}_{,\tilde{x}}$ and micro-scale kinematic measure $\tilde{\psi}_{11}$ have non-equal

values on the boundary, localized deformation energy density of finite thickness near that boundary is observed, while the deformation energy density in the rest of the domain of the problem is rather uniform. Second, for fixed macro-scale displacement $\tilde{\tilde{\phi}}$ applied at both boundaries and imposed double traction or micro-scale kinematic measure $\tilde{\psi}_{11}$ at one end, we notice both compression and tension (negative and positive macro-scale displacement gradient $\tilde{\tilde{\phi}}_{,\tilde{x}}$) induced within the granular structure. Third, the gradients appearing because of the imposed field variables $\tilde{\tilde{\phi}}$ and $\tilde{\psi}_{11}$ at both ends only exist close to the outer boundaries of the structure, thereby signifying the existence of boundary layers. Finally, one notices the small change in the macro-scale displacement $\tilde{\tilde{\phi}}$ in response to the alterations in the imposed non-classical boundary conditions. Nevertheless, such small changes have large influence on the energy localization near the boundaries, and such energy localization becomes even more noticeable as the size of the rod shrinks.

3.5. Parametric study

To further explore the effect of the material constants α_m, α_{Mm}, and l_s on the behavior of the field variables $\tilde{\tilde{\phi}}$ and $\tilde{\psi}_{11}$, a parametric study is performed. We consider two cases of boundary conditions for this investigation. Fig. 6 shows the results for the following applied boundary conditions

$$\tilde{\tilde{\phi}}(0)=0, \quad \tilde{\psi}_{11}(0)=0, \quad \tilde{\tilde{\phi}}(1)=0.01, \quad \tilde{\psi}_{11}(1)=0, \tag{42}$$

and Fig. 7 shows the results for the following boundary conditions

$$\tilde{\tilde{\phi}}(0)=0, \quad \tilde{\psi}_{11}(0)=0, \quad \tilde{\tilde{\phi}}(1)=0, \quad \tilde{\psi}_{11}(1)=0.01. \tag{43}$$

In both studies, the baseline material constants are taken as $\alpha_m = 0.5$, $\alpha_{Mm} = -0.4$ and $l_s = 0.05$. In Fig. 6(a) and Fig. 7(a) the material constant α_m is varied, in Fig. 6(b) and Fig. 7(b) the material constant α_{Mm} is varied, and in Fig. 6(c) and Fig. 7(c) the material constant l_s is varied. We here

recognize that a growth in the material constant l_s can be interpreted as either an increase in the second gradient stiffness of the material, or as a decrease in the size of the rod under study.

For the case of boundary conditions in Eq. (42) with the results shown in Fig. 6, a change in the values of the parameters α_m, α_{Mm}, and l_s has small effect on the solution for the macro-scale displacement $\tilde{\tilde{\phi}}$. However, it is evident that increasing α_m or α_{Mm} alters the solution for $\tilde{\psi}_{11}$ significantly. Moreover, increasing α_m and α_{Mm}, decreases and increases the size of the boundary layer, respectively. An increase in the value of l_s reduces the maximum for $\tilde{\psi}_{11}$ and increases the size of the boundary layer. The change of the size of the boundary layer due the value of the parameter l_s may be explained using the definition of the parameter κ. A larger value for the parameter l_s results in smaller value for κ which consequently leads to larger boundary layer.

For the case of the boundary conditions in Eq. (43) with the results shown in Fig. 7, increasing α_m results in a change from positive to negative sign for the macro-scale displacement $\tilde{\tilde{\phi}}$, which switches the regions of compression and tension (see Fig. 7(a)). According to Fig. 7(a), the micro-scale kinematic measure $\tilde{\psi}_{11}$ follows the same trend, although the sign of the solution for $\tilde{\psi}_{11}$ becomes negative as α_m increases while the boundary layer thickness decreases somewhat. Fig. 7(b) shows the results for the change in the value of α_{Mm}. Increasing α_{Mm} also changes the sign of the macro-scale displacement $\tilde{\tilde{\phi}}$. Furthermore, as the value of α_{Mm} increases, the boundary layer size increases by a small amount. Fig. 7(c) shows that increasing l_s results in an increase in the magnitude of the macro-scale displacement $\tilde{\tilde{\phi}}$ as well as an increase in the size of the boundary layer.

The size effect of the rod can be observed in Fig. 6(c) and Fig. 7(c), where a decrease in the size of the sample (increase in the value of l_s) results in a larger boundary layer which implies that the localization zone of the strain energy has grown and spread towards the center of the rod. In this case, the average deformation energy density absorbed by the material has increased compared to the same material with larger size, thus suggesting a stiffening effect.

4. Free vibration behavior

4.1. General solution

In this section, we analyze the free vibration characteristics of the 1D granular rod. The dimensionless form of the governing equations of motion are stated in Eq. (27) with the boundary conditions expressed in Eq. (28). For small harmonic vibration, the following form of solution (plane wave solution) is assumed

$$\tilde{\bar{\phi}}\left(\tilde{x},\tilde{t}\right)=\bar{\Phi}\left(\tilde{x}\right)e^{i\omega\tilde{t}},\quad \tilde{\psi}_{11}\left(\tilde{x},\tilde{t}\right)=\Psi\left(\tilde{x}\right)e^{i\omega\tilde{t}}, \tag{44}$$

where $\bar{\Phi}$ and Ψ are the dimensionless space parts of the solutions and ω is the dimensionless angular natural frequency. Substitution of Eq. (44) into the governing equations of motion in Eq. (27) results in the following equations

$$\left(1+\alpha_m+2\alpha_{Mm}\right)\bar{\Phi}_{,\tilde{x}\tilde{x}}-\left(\alpha_m+\alpha_{Mm}\right)\Psi_{,\tilde{x}}=-\omega^2\bar{\Phi}, \tag{45a}$$

$$l_s^2\Psi_{,\tilde{x}\tilde{x}}+\left(\alpha_m+\alpha_{Mm}\right)\bar{\Phi}_{,\tilde{x}}-\alpha_m\Psi=-\frac{\omega^2}{12n^2}\Psi+\frac{\omega^2}{80n^4}\Psi_{,\tilde{x}\tilde{x}}. \tag{45b}$$

The above equations can be uncoupled to obtain two fourth order homogenous linear ordinary differential equations with constant coefficients as follows

$$z_1\bar{\Phi}_{,\tilde{x}\tilde{x}\tilde{x}\tilde{x}}+z_2\bar{\Phi}_{,\tilde{x}\tilde{x}}+z_3\bar{\Phi}=0, \tag{46a}$$

$$z_1\Psi_{,\tilde{x}\tilde{x}\tilde{x}\tilde{x}}+z_2\Psi_{,\tilde{x}\tilde{x}}+z_3\Psi=0, \tag{46b}$$

where

$$\begin{aligned}
z_1&=3\left(\omega^2-80l_s^2n^4\right)\left(1+\alpha_m+2\alpha_{Mm}\right),\\
z_2&=240n^4\left(\alpha_m-\alpha_{Mm}^2-l_s^2\omega^2\right)-20n^2\omega^2\left(1+\alpha_m+2\alpha_{Mm}\right)+3\omega^4,\\
z_3&=20n^2\omega^2\left(12\alpha_m n^2-\omega^2\right).
\end{aligned} \tag{47}$$

The general solutions for the differential equations in Eq. (46) can be presented as

$$\bar{\Phi}=\hat{\bar{\Phi}}_1\cos\left(k_1\tilde{x}\right)+\hat{\bar{\Phi}}_2\sin\left(k_1\tilde{x}\right)+\hat{\bar{\Phi}}_3\cosh\left(k_2\tilde{x}\right)+\hat{\bar{\Phi}}_4\sinh\left(k_2\tilde{x}\right), \tag{48a}$$

$$\Psi = \hat{\Psi}_1 \cos\left(k_1 \tilde{x}\right) + \hat{\Psi}_2 \sin\left(k_1 \tilde{x}\right) + \hat{\Psi}_3 \cosh\left(k_2 \tilde{x}\right) + \hat{\Psi}_4 \sinh\left(k_2 \tilde{x}\right), \tag{48b}$$

where

$$k_1 = \left(\frac{z_2 - \sqrt{z_2^2 - 4 z_1 z_3}}{2 z_1} \right)^{\frac{1}{2}}, \quad k_2 = \left(\frac{-z_2 - \sqrt{z_2^2 - 4 z_1 z_3}}{2 z_1} \right)^{\frac{1}{2}}. \tag{49}$$

In Eq. (48), k_1 and k_2 are the dimensionless angular wavenumbers, and are functions of the material parameters and the angular frequency ω. Also, $\hat{\bar{\Phi}}_i, \hat{\Psi}_i, i = 1, \ldots, 4$ are constant to be determined by the appropriate boundary conditions, which, using Eq. (45a), are related as

$$\begin{aligned} &\hat{\Psi}_1 = \alpha \hat{\bar{\Phi}}_2, \quad \hat{\Psi}_2 = -\alpha \hat{\bar{\Phi}}_1, \quad \text{where} \quad \alpha = \frac{\left(1 + \alpha_m + 2\alpha_{Mm}\right) k_1^2 - \omega^2}{\left(\alpha_m + \alpha_{Mm}\right) k_1}, \\ &\hat{\Psi}_3 = \beta \hat{\bar{\Phi}}_4, \quad \hat{\Psi}_4 = \beta \hat{\bar{\Phi}}_3 \qquad \text{where} \quad \beta = \frac{\left(1 + \alpha_m + 2\alpha_{Mm}\right) k_2^2 + \omega^2}{\left(\alpha_m + \alpha_{Mm}\right) k_2}. \end{aligned} \tag{50}$$

In what follows, we study the free vibration characteristics of the 1D granular rod subjected to four types of boundary conditions. The first three types of boundary conditions are examined following the same motivation discussed in the static case: for identical classical boundary conditions, how does a change in the non-classical boundary conditions affect the response of the system. The fourth type of boundary conditions is investigated to have a more complete comparison with the results of the models found in the literature. For the analyses to follow, we consider the same material constants as for the static case, namely, $\alpha_m = 0.5$, $\alpha_{Mm} = -0.4$, $l_s = 0.05$, and $n = 100$, and compare the resulting natural frequencies and mode shapes with the solutions of a classical rod problem. We note that, in the following results, the mode shapes of the classical rod have been scaled such that they have the same amplitude as the macro-scale displacement $\tilde{\bar{\phi}}$ amplitude for the mode shapes of the present model.

4.2. Clamped strained-clamped strained (CS-CS)

The boundary conditions associated with the CS-CS case are defined as

$$\bar{\Phi}(0) = 0, \quad \Psi(0) = 0, \quad \bar{\Phi}(1) = 0, \quad \Psi(1) = 0. \tag{51}$$

Eq. (51) enforces that the macro-scale displacement $\tilde{\tilde{\phi}}$ and the micro-scale kinematic measure $\tilde{\psi}_{11}$ are identically fixed at both ends. Enforcing Eq. (51), and by using Eq. (50), the following set of algebraic equations result from Eq. (48)

$$\begin{bmatrix} 1 & 0 & 1 & 0 \\ 0 & \alpha & 0 & \beta \\ \cos(k_1) & \sin(k_1) & \cosh(k_2) & \sinh(k_2) \\ -\alpha\sin(k_1) & \alpha\cos(k_1) & \beta\sinh(k_2) & \beta\cosh(k_2) \end{bmatrix} \begin{Bmatrix} \hat{\tilde{\Phi}}_1 \\ \hat{\tilde{\Phi}}_2 \\ \hat{\tilde{\Phi}}_3 \\ \hat{\tilde{\Phi}}_4 \end{Bmatrix} = \begin{Bmatrix} 0 \\ 0 \\ 0 \\ 0 \end{Bmatrix}. \tag{52}$$

The necessary condition to have non-zero solutions for Eq. (52) is that the determinant of the coefficient matrix is zero, i.e.

$$\left(\alpha^2 - \beta^2\right)\sin(k_1)\sinh(k_2) + 2\alpha\beta\left(\cos(k_1)\cosh(k_2) - 1\right) = 0. \tag{53}$$

Eq. (53) is a transcendental equation denoting the general characteristic equation for the CS-CS boundary conditions and is equivalent to the characteristic equation for the clamped-clamped case of the nonlocal strain gradient rod in [31] for $\alpha = k_1$ and $\beta = k_2$.

Fig. 8(a-c) show the first three mode shapes and natural frequencies. The mode shapes corresponding to the macro-scale displacement $\tilde{\tilde{\phi}}$ are similar to that's for the classical one-dimensional continua for the material parameters considered here. Denoting by ω_i and ω_i^c, respectively, the i^{th} natural frequency of the current model and the classical continuum model, the first three natural frequencies in the CS-CS boundary condition case for the chosen material parameters are smaller than their classical continuum counterparts and are evaluated as $\omega_1 = 0.8283\omega_1^c$, $\omega_2 = 0.8290\omega_2^c$, and $\omega_3 = 0.8300\omega_3^c$.

4.3. Clamped strained-clamped forcing (CS-CF)

The boundary conditions associated with the CS-CF case are obtained by having the macro-scale displacement $\tilde{\tilde{\phi}}$ at both ends fixed, the micro-scale kinematic measure $\tilde{\psi}_{11}$ fixed at the left end, and the double traction zero (free) at the right end. Explicitly, the boundary conditions are stated as

$$\bar{\Phi}(0)=0,\quad \Psi(0)=0,\quad \bar{\Phi}(1)=0,\quad \Psi_{,\tilde{x}}(1)=0, \tag{54}$$

where the last condition is obtained by introducing the solution in Eq. (44) into the boundary condition in Eq. (28b). Enforcing Eq. (54), and by using Eq. (50), the following set of algebraic equations result from Eq. (48)

$$\begin{bmatrix} 1 & 0 & 1 & 0 \\ 0 & \alpha & 0 & \beta \\ \cos(k_1) & \sin(k_1) & \cosh(k_2) & \sinh(k_2) \\ -\alpha k_1 \cos(k_1) & -\alpha k_1 \sin(k_1) & \beta k_2 \cosh(k_2) & \beta k_2 \sinh(k_2) \end{bmatrix} \begin{Bmatrix} \hat{\bar{\Phi}}_1 \\ \hat{\bar{\Phi}}_2 \\ \hat{\bar{\Phi}}_3 \\ \hat{\bar{\Phi}}_4 \end{Bmatrix} = \begin{Bmatrix} 0 \\ 0 \\ 0 \\ 0 \end{Bmatrix}. \tag{55}$$

The characteristic equation corresponding to Eq. (55) is

$$(\alpha k_1 + \beta k_2)\left[\alpha \cos(k_1)\sinh(k_2) - \beta \sin(k_1)\cosh(k_2)\right] = 0. \tag{56}$$

Eq. (56) is the general characteristic equation for the CS-CF boundary conditions and for $\alpha = k_1$ and $\beta = k_2$ it becomes equivalent to the characteristic equation for the clamped-simply supported case of the nonlocal strain gradient rod described in [31].

Fig. 8(d-f) show the first three mode shapes and natural frequencies. Similar to the results for the CS-CS case, the mode shapes corresponding to the macro-scale displacement $\tilde{\tilde{\phi}}$ for the CS-CF case are approximately same as the mode shapes of classical 1D bar. The first three natural frequencies in the CS-CF boundary condition case are smaller than their classical continuum counterparts for the material parameters considered here, and have values of $\omega_1 = 0.8267\omega_1^c$, $\omega_2 = 0.8278\omega_2^c$, and $\omega_3 = 0.8292\omega_3^c$, respectively.

4.4. Clamped forcing-clamped forcing (CF-CF)

The boundary conditions associated with the CF-CF case are expressed as

$$\bar{\Phi}(0)=0,\quad \Psi_{,\tilde{x}}(0)=0,\quad \bar{\Phi}(1)=0,\quad \Psi_{,\tilde{x}}(1)=0. \tag{57}$$

Enforcing the boundary conditions in Eq. (57), the following set of algebraic equations result from Eq. (48)

$$\begin{bmatrix} 1 & 0 & 1 & 0 \\ -\alpha k_1 & 0 & \beta k_2 & 0 \\ \cos(k_1) & \sin(k_1) & \cosh(k_2) & \sinh(k_2) \\ -\alpha k_1 \cos(k_1) & -\alpha k_1 \sin(k_1) & \beta k_2 \cosh(k_2) & \beta k_2 \sinh(k_2) \end{bmatrix} \begin{Bmatrix} \hat{\bar{\Phi}}_1 \\ \hat{\bar{\Phi}}_2 \\ \hat{\bar{\Phi}}_3 \\ \hat{\bar{\Phi}}_4 \end{Bmatrix} = \begin{Bmatrix} 0 \\ 0 \\ 0 \\ 0 \end{Bmatrix}. \tag{58}$$

The characteristic equation corresponding to Eq. (58) is

$$(\alpha k_1 + \beta k_2)^2 \sin(k_1) \sinh(k_2) = 0. \tag{59}$$

Eq. (59) is the general characteristic equation for the CF-CF boundary conditions, and for $\alpha = k_1$ and $\beta = k_2$, it becomes of similar form to the characteristic equation for the simply supported-simply supported case of the nonlocal strain gradient rod in [31], the nonlocal strain gradient rod in [27], and the strain gradient rod in [30].

Fig. 8(g-i) show the first three mode shapes and natural frequencies. Similar to previous cases, the mode shapes corresponding to the macro-scale displacement $\tilde{\tilde{\phi}}$ for the CF-CF case are similar to that of the classical 1D continua. The first three natural frequencies in the CF-CF boundary condition case are smaller than their classical continuum counterparts for the material parameters chosen in this study, and have values of $\omega_1 = 0.8252\omega_1^c$, $\omega_2 = 0.8266\omega_2^c$, and $\omega_3 = 0.8283\omega_3^c$, respectively.

4.5. Clamped forcing-free strained (CF-FS)

The boundary conditions associated with the CF-FS case are expressed as

$$\bar{\Phi}(0) = 0, \quad \Psi_{,\tilde{x}}(0) = 0, \quad \bar{\Phi}_{,\tilde{x}}(1) = 0, \quad \Psi(1) = 0. \tag{57}$$

With regards to Eq. (57), Eq. (48) results in the following set of algebraic equations

$$\begin{bmatrix} 1 & 0 & 1 & 0 \\ -\alpha k_1 & 0 & \beta k_2 & 0 \\ -k_1 \sin(k_1) & k_1 \cos(k_1) & k_2 \sinh(k_2) & k_2 \cosh(k_2) \\ -\alpha \sin(k_1) & \alpha \cos(k_1) & \beta \sinh(k_2) & \beta \cosh(k_2) \end{bmatrix} \begin{Bmatrix} \hat{\bar{\Phi}}_1 \\ \hat{\bar{\Phi}}_2 \\ \hat{\bar{\Phi}}_3 \\ \hat{\bar{\Phi}}_4 \end{Bmatrix} = \begin{Bmatrix} 0 \\ 0 \\ 0 \\ 0 \end{Bmatrix}. \tag{58}$$

The characteristic equation corresponding to Eq. (58) is

$$(\alpha k_1 + \beta k_2)(\alpha k_2 - \beta k_1)\cos(k_1)\cosh(k_2) = 0. \tag{59}$$

Eq. (59) is the general characteristic equation for the CF-FS boundary conditions and for $\alpha = k_1$ and $\beta = k_2$ it becomes of similar form to the characteristic equation for the CF-FS case of the nonlocal strain gradient rod in [27].The first three natural frequencies for the CF-FS case are $\omega_1 = 0.8247\omega_1^c$, $\omega_2 = 0.8258\omega_2^c$, and $\omega_3 = 0.8275\omega_3^c$, respectively, which are lower than classical continuum predictions for the material parameters considered. In addition, the macro-scale displacement $\tilde{\bar{\phi}}$ mode shapes are close to the classical continuum predictions.

Based on the results of the four different examples studied above, several observations and conclusions can be made. Firstly, the mode shapes of the macro-scale displacement $\tilde{\bar{\phi}}$ are similar to that of a classical continuum, although for a different choice of material parameters (for example if we had $\alpha_{Mm} = 0$), small deviations from the mode shapes of classical rod are observed (results not shown). Such a deviation is the result of the presence of terms containing the second wavenumber k_2 in Eq. (48), which, for the problems studied here, had negligible amplitude compared to the leading term containing k_1. Moreover, one concludes from the first three visited examples that even when the double traction is prescribed as zero on the boundaries, the microstructural effects alter the natural frequency of the system. This is in contradistinction to the results from the static problem where a classical form of solution is obtained if the non-classical terms are not excited. This distinction in the behavior of the system in static and dynamic problems are due to the presence of the terms containing dynamic length scales in the governing equations of motion.

4.6.Parametric study

In order to study the effect of different material constants on the dynamic behavior of one-dimensional materials with granular microstructure, we have plotted the ratio of the first three natural frequencies for the three CS-CS, CS-CF, and CF-CF cases to their classical counterparts for different material parameters with the base material constants at $\alpha_m = 0.5$, $\alpha_{Mm} = 0$, $l_s = 0.05$, and $n = 100$ in Fig. 9. Based on the results in Fig. 9, the following conclusions can be drawn. First, an increase in the micro-scale (relative deformation) stiffness, α_m, leads to larger natural frequencies (Fig. 9(a)). This result is expected as additional stiffness increases the natural frequency of the system. Second, contrary to the trend observed for the effect of the parameter α_m, an increase in the cross-linking stiffness α_{Mm} is accompanied by an initial increase in the value of the natural frequencies, followed by a decrease (Fig. 9(b)). Therefore, the effect of the parameter α_{Mm} can be either softening or stiffening. Third, increasing the length scale parameter l_s results in an increase in the value of the natural frequencies (Fig. 9(f)), hence implying stiffening of the material when either the second gradient stiffness becomes larger or when the rod size becomes smaller. For l_s values large enough, an asymptotic value for the natural frequencies are obtained. Similar observation has been made for the rod modeled using nonlocal strain gradient theory [31]. Fourth, the natural frequencies can be smaller or larger than their classical counterparts, depending on the material constants. Fifth, one observes that the effect of different boundary conditions on the natural frequencies is rather small for a wide range of material parameters. For higher modes, however, the effect of different boundary conditions on the results becomes increasingly significant. Finally, it is interesting to note that the higher mode frequencies are not integer multiples of the fundamental mode, which is a departure from the results for classical 1D elastic rod under the considered boundary conditions, and seems to suggest an apparent internal damping.

5. Conclusion and Summary (prognosis towards experimental design)

Mechanical response of materials with granular microstructures are known to be influenced by the grain-scale mechano-morphology. Here we have utilized the granular micromechanics approach (GMA) based continuum theory to reveal certain peculiar aspects of the mechanical behavior of a material with granular microstructure. To keep the development tractable and understandable, we

have focused upon a 1D rod composed of granular materials. To this end, the governing equations of motion and the variationally consistent boundary conditions for a one-dimensional material with granular microstructure were obtained using the principle of least action. Closed-form solutions for both the static and dynamic problems were obtained and the effect of different boundary conditions and material parameters on the response of the material were investigated. The key findings of the presented work are:

1. That micromorphicity due to micro-mechano-morphological properties has a significant influence on the static and free vibration response of rods with granular microstructure.
2. In the static case, we observe that the dependency of the structural response on the imposed boundary conditions is most obvious near the boundaries of the structure where gradients of strain are large. In addition, the size-dependency effects are manifested in the width of the emergent boundary layers.
3. In the dynamic case, the length scale parameter has stiffening effect, i.e., as the size of the structure shrinks, the behavior is predicted to be stiffer, a finding which classical theory does not predict.
4. The mode shapes corresponding to the micro-scale kinematic measure $\tilde{\psi}_{11}$ are not identical to that of the macro-scale displacement gradient $\tilde{\tilde{\phi}}_{,\tilde{x}}$, as distinct from that for a second gradient model and account for the energy due to the relative deformation in macro- and micro-scales.
5. Additional kinematic constraints and simplifications imposed on the presented model leads to several (nonlocal) strain gradient models introduced in the literature, and therefore, the current model, encompasses such models as special cases.
6. While the cases studied in the static problem show microstructural effects of the system under certain boundary conditions, the effect of the microstructure is always present in the dynamic problem for any form of applied boundary conditions.
7. The dynamic length scale parameters (referred to as nonlocal parameters in the literature) in the current model are directly linked to the micro-scale mass density distribution of the system under study and do not take arbitrary values.
8. The model predicts measureable effects such that experimental approaches/protocols can be designed to detect these effects.

9. While a 1D system is helpful in understanding the underlying physics behind the observed phenomena, many engineering applications are concerned with higher dimensional systems. GMA based micromorphic model of degree one presented here can be systematically expanded to include 2D and 3D systems [41], or to model deflection in beams [61].

To conclude, appreciating the complexity of the materials with granular microstructure and the limitations on the current experimental prescriptions to observe and extract microstructural effects, the results of the current paper can promote the understanding of such complex systems and what to expect if experiments are to be devised. Furthermore, the results of the current paper will serve as a prelude to our future work on static deformation, vibration and elastic wave propagation simulations of initial/boundary value problems for structures made of granular media.

Statement of Competing Interest

Authors have no competing interests to declare.

Acknowledgements

This research is supported in part by the United States National Science Foundation grant CMMI -1727433.

References

[1] Barchiesi E, dell'Isola F, Laudato M, Placidi L, Seppecher P. A 1D continuum model for beams with pantographic microstructure: asymptotic micro-macro identification and numerical results. In: *Advanced Structured Materials*. Springer Verlag, pp. 43–74.

[2] Del Vescovo D, Giorgio I. Dynamic problems for metamaterials: Review of existing models and ideas for further research. *Int J Eng Sci* 2014; 80: 153–172.

[3] Barchiesi E. Multi-scale and multi-physics: towards next-generation engineering materials. *Continuum Mechanics and Thermodynamics* 2020; 32: 541–554.

[4] Gonella S, Steven Greene M, Liu WK. Characterization of heterogeneous solids via wave methods in computational microelasticity. *J Mech Phys Solids* 2011; 59: 959–974.

[5] Lam DCC, Yang F, Chong ACM, Wang J, Tong P. Experiments and theory in strain gradient elasticity. *J Mech Phys Solids* 2003; 51: 1477–1508.

[6] Rosi G, Auffray N, Combescure C. On the failure of classic elasticity in predicting elastic wave propagation in gyroid lattices for very long wavelengths. *Symmetry* 2020; 12(8): 1243.

[7] Sun L, Han RPS, Wang J, Lim CT. Modeling the size-dependent elastic properties of polymeric nanofibers. *Nanotechnology* 2008; 19: 455706.

[8] Berezovski A, Engelbrecht J, Salupere A, Tamm K, Peets T, Berezovski M. Dispersive waves in microstructured solids. *Int J Solids Struct* 2013; 50: 1981–1990.

[9] Eringen AC. *Microcontinuum Field Theories*. Springer New York, 1999.

[10] Eringen AC, Edelen DGB. On nonlocal elasticity. *Int J Eng Sci* 1972; 10: 233–248.

[11] Eringen AC. Plane waves in nonlocal micropolar elasticity. *Int J Eng Sci* 1984; 22: 1113–1121.

[12] Mindlin RD. Micro-structure in linear elasticity. *Arch Ration Mech Anal* 1964; 16: 51–78.

[13] Germain P. The Method of Virtual Power in Continuum Mechanics. Part 2: Microstructure. *SIAM J Appl Math* 1973; 25: 556–575.

[14] Toupin RA. Theories of elasticity with couple-stress. *Arch Ration Mech Anal* 1964; 17: 85–112.

[15] Challamel N, Wang CM, Elishakoff I. Nonlocal or gradient elasticity macroscopic models: A question of concentrated or distributed microstructure. *Mech Res Commun* 2016; 71: 25–31.

[16] Seppecher P, Alibert JJ, Isola FD. Linear elastic trusses leading to continua with exotic mechanical interactions. In: *Journal of Physics: Conference Series* 2011 Sep 15 (Vol. 319, No. 1, p. 012018). IOP Publishing.

[17] Barretta R, Faghidian SA, Luciano R. Longitudinal vibrations of nano-rods by stress-driven integral elasticity. *Mech Adv Mater Struct* 2019; 26: 1307–1315.

[18] Chang CS, Gao J. Wave Propagation in Granular Rod Using High-Gradient Theory. *J Eng Mech* 1997; 123: 52–59.

[19] Zhu X, Li L. Closed form solution for a nonlocal strain gradient rod in tension. *Int J Eng Sci* 2017; 119: 16–28.

[20] Ayad M, Karathanasopoulos N, Ganghoffer JF, Lakiss H. Higher-gradient and micro-inertia contributions on the mechanical response of composite beam structures. *Int J Eng Sci* 2020; 154:

103318.

[21] Dontsov E V., Tokmashev RD, Guzina BB. A physical perspective of the length scales in gradient elasticity through the prism of wave dispersion. *Int J Solids Struct* 2013; 50: 3674–3684.

[22] Güven U. A generalized nonlocal elasticity solution for the propagation of longitudinal stress waves in bars. *Eur J Mech A/Solids* 2014; 45: 75–79.

[23] Papargyri-Beskou S, Beskos D. Static analysis of gradient elastic bars, beams, plates and shells. *Open Mech J* 2010; 4: 65–73.

[24] De Domenico D, Askes H, Aifantis EC. Discussion of "Derivation of Mindlin's first and second strain gradient elastic theory via simple lattice and continuum models" by Polyzos and Fotiadis. *International Journal of Solids and Structures* 2020; 191–192: 646–651.

[25] Tsepoura KG, Papargyri-Beskou S, Polyzos D, Beskos DE. Static and dynamic analysis of a gradient-elastic bar in tension. *Arch Appl Mech* 2002; 72: 483–497.

[26] Adhikari S, Murmu T, McCarthy MA. Dynamic finite element analysis of axially vibrating nonlocal rods. *Finite Elem Anal Des* 2013; 63: 42–50.

[27] Li L, Hu Y, Li X. Longitudinal vibration of size-dependent rods via nonlocal strain gradient theory. *Int J Mech Sci* 2016; 115–116: 135–144.

[28] Aydogdu M. Axial vibration of the nanorods with the nonlocal continuum rod model. *Phys E Low-Dimensional Syst Nanostructures* 2009; 41: 861–864.

[29] Numanoğlu HM, Akgöz B, Civalek Ö. On dynamic analysis of nanorods. *Int J Eng Sci* 2018; 130: 33–50.

[30] Kahrobaiyan MH, Asghari M, Ahmadian MT. Longitudinal behavior of strain gradient bars. *Int J Eng Sci* 2013; 66–67: 44–59.

[31] Xu XJ, Zheng ML, Wang XC. On vibrations of nonlocal rods: Boundary conditions, exact solutions and their asymptotics. *Int J Eng Sci* 2017; 119: 217–231.

[32] Benvenuti E, Simone A. One-dimensional nonlocal and gradient elasticity: Closed-form solution and size effect. *Mech Res Commun* 2013; 48: 46–51.

[33] Challamel N, Zhang Z, Wang CM. Nonlocal equivalent continua for buckling and vibration analyses of microstructured beams. *J Nanomechanics Micromechanics* 2015; 5: A4014004.

[34] Rahmani O, Pedram O. Analysis and modeling the size effect on vibration of functionally graded nanobeams based on nonlocal Timoshenko beam theory. *Int J Eng Sci* 2014; 77: 55–70.

[35] Fafalis DA, Filopoulos SP, Tsamasphyros GJ. On the capability of generalized continuum theories to capture dispersion characteristics at the atomic scale. *Eur J Mech A/Solids* 2012; 36: 25–37.

[36] Darban H, Luciano R, Caporale A, Fabbrocino F. Higher modes of buckling in shear deformable nanobeams. *Int J Eng Sci* 2020; 154: 103338.

[37] Numanoğlu HM, Civalek Ö. On the dynamics of small-sized structures. *Int J Eng Sci* 2019; 145: 103164.

[38] Andreaus U, dell'Isola F, Giorgio I, Placidi L, Lekszycki T, Rizzi NL. Numerical simulations of classical problems in two-dimensional (non) linear second gradient elasticity. *Int J Eng Sci* 2016; 108: 34–50.

[39] Farajpour A, Howard CQ, Robertson WSP. On size-dependent mechanics of nanoplates. *Int J Eng Sci* 2020; 156: 103368.

[40] Yang H, Müller WH. Size effects of mechanical metamaterials: a computational study based on a second-order asymptotic homogenization method. *Arch Appl Mech* 2020; 1–17.

[41] Nejadsadeghi N, Misra A. Extended granular micromechanics approach: a micromorphic theory of degree n. *Math Mech Solids* 2020; 25: 407–429.

[42] Misra A, Poorsolhjouy P. Granular micromechanics based micromorphic model predicts frequency band gaps. *Contin Mech Thermodyn* 2016; 28: 215–234.

[43] Misra A, Nejadsadeghi N. Longitudinal and transverse elastic waves in 1D granular materials modeled as micromorphic continua. *Wave Motion* 2019; 90: 175–195.

[44] Nejadsadeghi N, Placidi L, Romeo M, Misra A. Frequency band gaps in dielectric granular metamaterials modulated by electric field. *Mech Res Commun* 2019 ;95:96-103.

[45] Nejadsadeghi N, Misra A. Role of higher-order inertia in modulating elastic wave dispersion in materials with granular microstructure. *Int J Mech Sci* 2020; 185: 105867.

[46] Zeng X, Chen Y, Lee JD. Determining material constants in nonlocal micromorphic theory through phonon dispersion relations. *Int J Eng Sci* 2006; 44: 1334–1345.

[47] Chen Y, Lee JD. Connecting molecular dynamics to micromorphic theory.(I). Instantaneous and averaged mechanical variables. *Phys A Stat Mech its Appl* 2003; 322: 359–376.

[48] Madeo A, Collet M, Miniaci M, Billon K, Ouisse M, Neff P. Modeling phononic crystals via the weighted relaxed micromorphic model with free and gradient micro-inertia. *J Elast* 2018; 130: 59–83.

[49] Misra A, Nejadsadeghi N, De Angelo M, Placidi L. Chiral metamaterial predicted by granular micromechanics: verified with 1D example synthesized using additive manufacturing. *Contin Mech Thermodyn* 2020; 32: 1497-1513.

[50] Giorgio I, dell'Isola F, Misra A. Chirality in 2D Cosserat media related to stretch-micro-rotation coupling with links to granular micromechanics. *Int J Solids Struct* 2020; 202: 28–38.

[51] Tan SH, Poh LH. Enriched homogenized model for viscoelastic plane wave propagation in periodic layered composites. *Adv Model Simul Eng Sci* 2020; 7: 4.

[52] Tan SH, Poh LH. Homogenized Gradient Elasticity Model for Plane Wave Propagation in Bilaminate Composites. *J Eng Mech* 2018; 144: 04018075.

[53] Misra A, Ouyang L, Chen J, Ching WY. Ab initio calculations of strain fields and failure patterns in silicon nitride intergranular glassy films. *Philosophical Magazine* 2007; 87(25): 3839-52.

[54] Charlotte M, Truskinovsky L. Towards multi-scale continuum elasticity theory. *Contin Mech Thermodyn* 2008; 20: 133–161.

[55] Charlotte M, Truskinovsky L. Lattice dynamics from a continuum viewpoint. *J Mech Phys Solids* 2012; 60: 1508–1544.

[56] Essén H. Average angular velocity. *Eur J Phys* 1993; 14: 201–205.

[57] Wang ZP, Sun CT. Modeling micro-inertia in heterogeneous materials under dynamic loading. *Wave Motion* 2002; 36: 473–485.

[58] Barchiesi E, Laudato M, Di Cosmo F. Wave dispersion in non-linear pantographic beams. *Mech Res Commun* 2018; 94: 128–132.

[59] De Domenico D, Askes H. A new multi-scale dispersive gradient elasticity model with micro-inertia: Formulation and C0-finite element implementation. *Int J Numer Methods Eng* 2016; 108: 485–512.

[60] Misra A, Poorsolhjouy P. Identification of higher-order elastic constants for grain assemblies based upon granular micromechanics. *Math Mech Complex Syst* 2015; 3: 285–308.

[61] Angelo M De, Placidi L, Nejadsadeghi N, Misra A. Non-standard Timoshenko beam model for chiral metamaterial: identification of stiffness parameters. *Mech Res Commun* 2019; 103462.

List of Figures

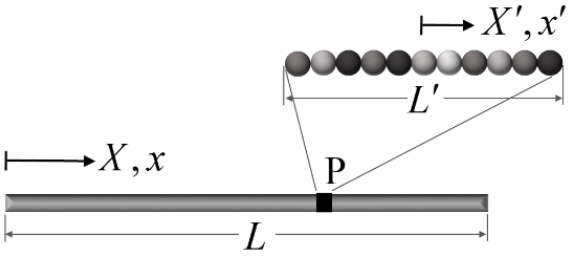

Fig 1. Schematic of a one-dimensional granular structure modeled as a one-dimensional continuum, and the material point P and its granular microstructure magnified for better visualization.

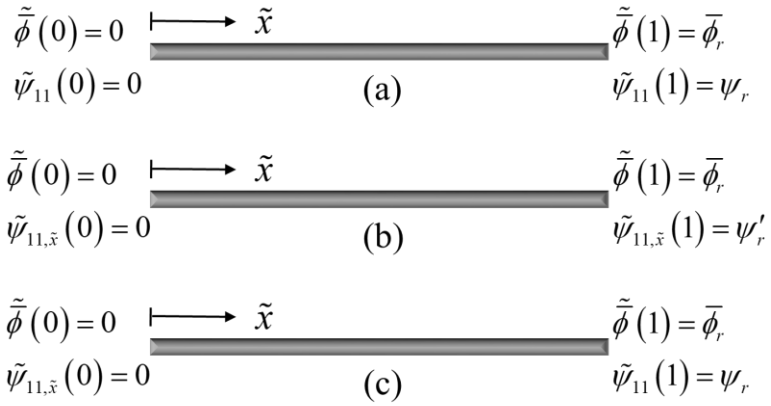

Fig 2. Schematic of the applied boundary conditions for the static problem describing the behavior of a 1D granular rod in (a) the first scenario, (b) the second scenario, and (c) the third scenario.

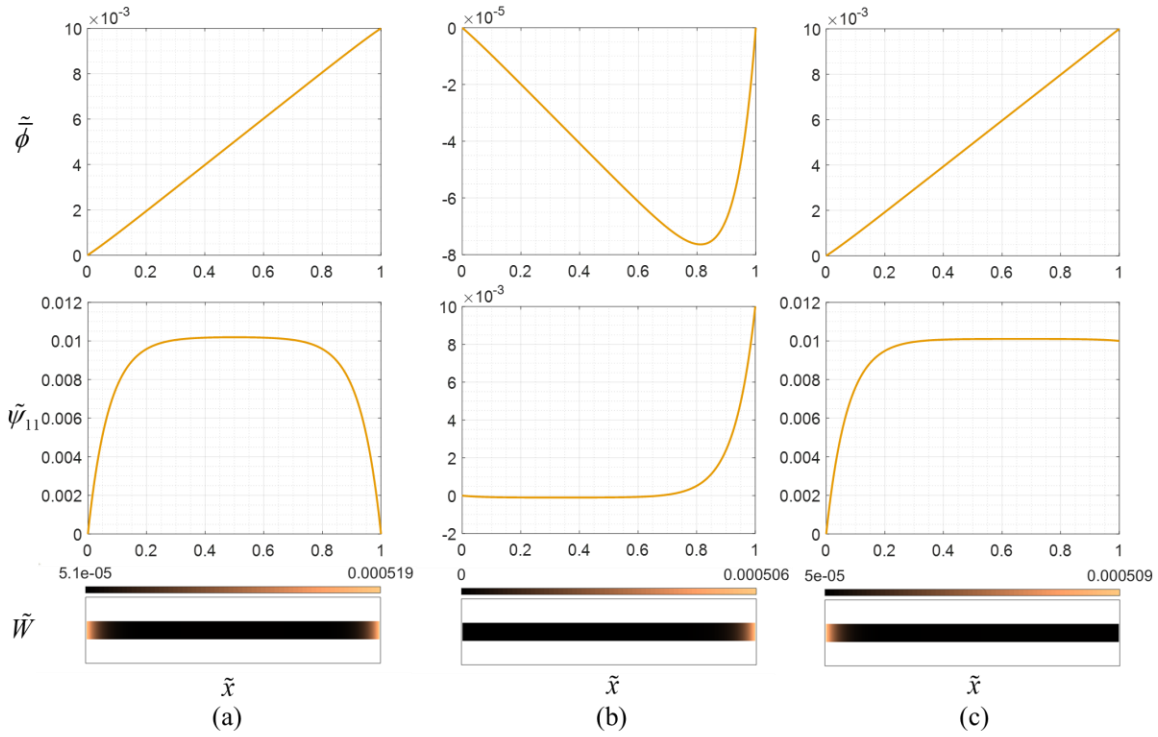

Fig 3. Results for the static behavior of a 1D granular rod with material constants $\alpha_m = 0.5$, $\alpha_{Mm} = -0.4$, and $l_s = 0.05$ with imposed boundary conditions (a) $\bar{\phi}_r = 0.01$ and $\psi_r = 0$, (b) $\bar{\phi}_r = 0$ and $\psi_r = 0.01$, and (c) $\bar{\phi}_r = 0.01$ and $\psi_r = 0.01$ in the first scenario.

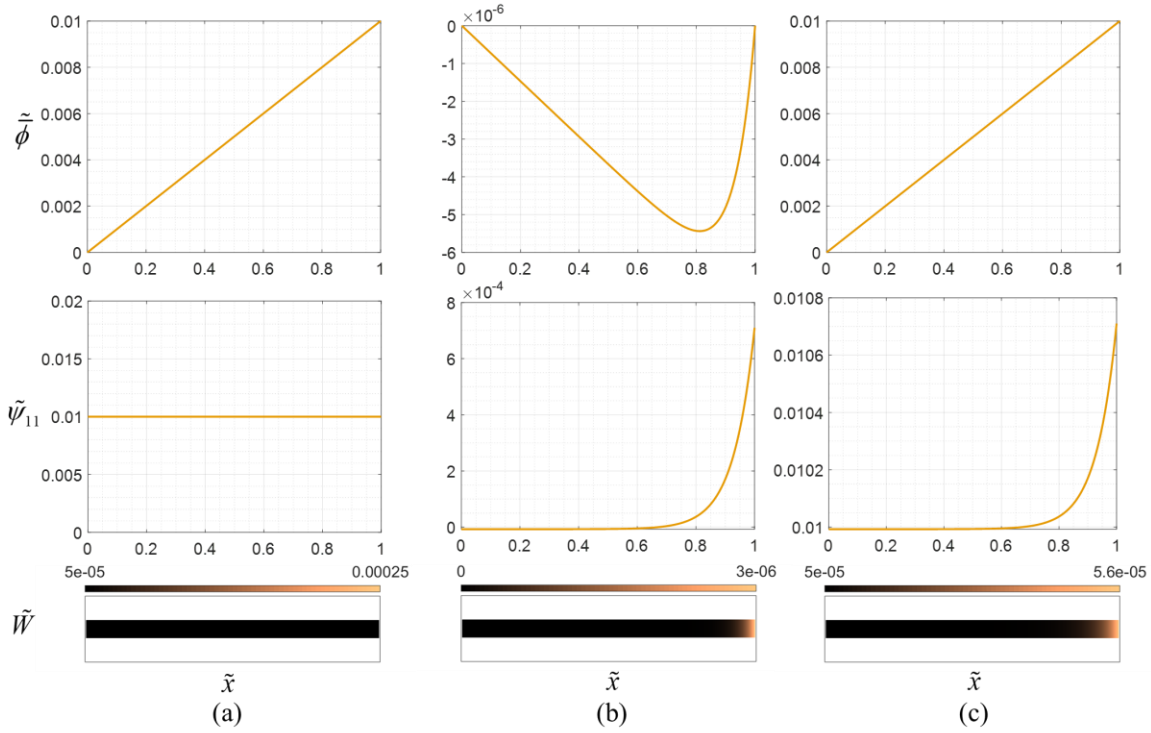

Fig 4. Results for the static behavior of a 1D granular rod with material constants $\alpha_m = 0.5$, $\alpha_{Mm} = -0.4$, and $l_s = 0.05$ with imposed boundary conditions (a) $\bar{\phi}_r = 0.01$ and $\psi'_r = 0$, (b) $\bar{\phi}_r = 0$ and $\psi'_r = 0.01$, and (c) $\bar{\phi}_r = 0.01$ and $\psi'_r = 0.01$ in the second scenario.

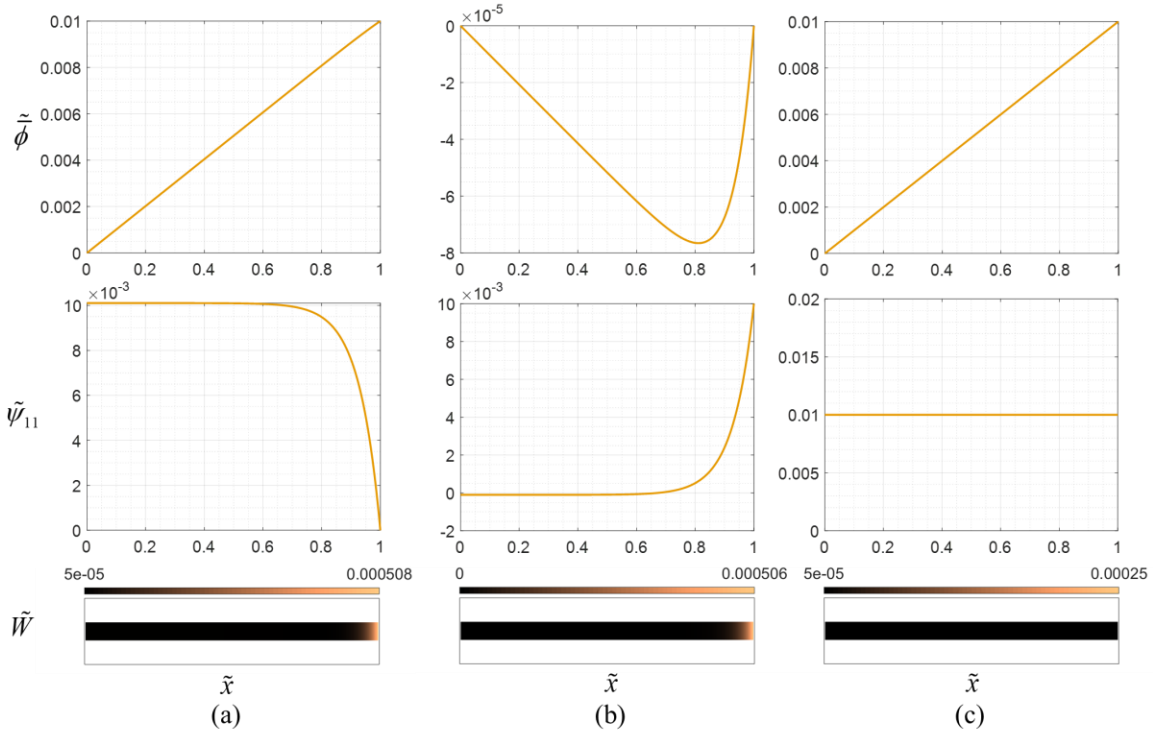

Fig 5. Results for the static behavior of a 1D granular rod with material constants $\alpha_m = 0.5$, $\alpha_{Mm} = -0.4$, and $l_s = 0.05$ with imposed boundary conditions (a) $\bar{\phi}_r = 0.01$ and $\psi_r = 0$, (b) $\bar{\phi}_r = 0$ and $\psi_r = 0.01$, and (c) $\bar{\phi}_r = 0.01$ and $\psi_r = 0.01$ in the third scenario.

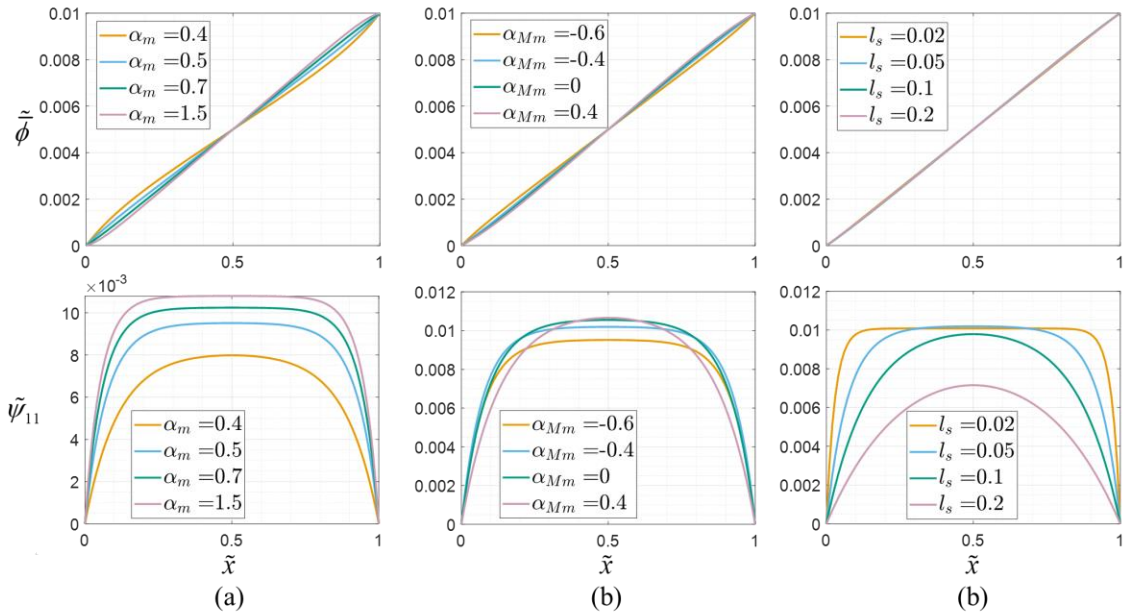

Fig 6. Results comparing the effect of the material constants (a) α_m, (b) α_{Mm}, and (c) l_s on the behavior of a 1D granular rod with material constants based at $\alpha_m = 0.5$, $\alpha_{Mm} = -0.4$, and $l_s = 0.05$, for the imposed boundary conditions $\tilde{\tilde{\phi}}(0) = \tilde{\psi}_{11}(0) = \tilde{\psi}_{11}(1) = 0, \quad \tilde{\tilde{\phi}}(1) = 0.01$.

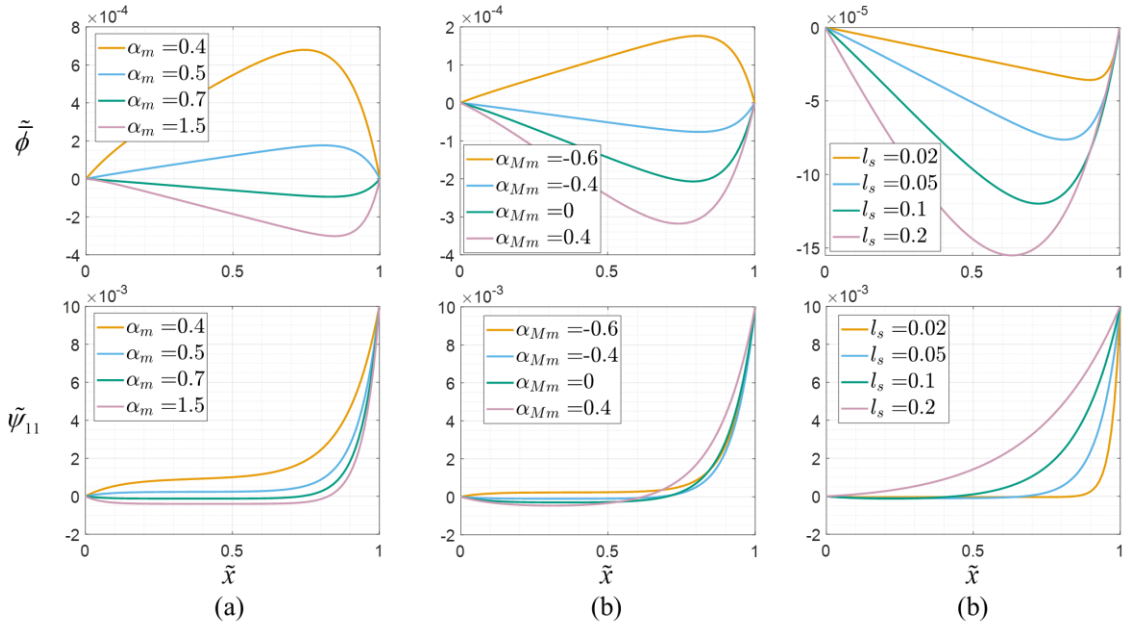

Fig 7. Results comparing the effect of the material constants (a) α_m, (b) α_{Mm}, and (c) l_s on the behavior of a 1D granular rod with material constants based at $\alpha_m = 0.5$, $\alpha_{Mm} = -0.4$, and $l_s = 0.05$, for the imposed boundary conditions $\tilde{\tilde{\phi}}(0) = \tilde{\psi}_{11}(0) = \tilde{\tilde{\phi}}(1) = 0, \quad \tilde{\psi}_{11}(1) = 0.01$.

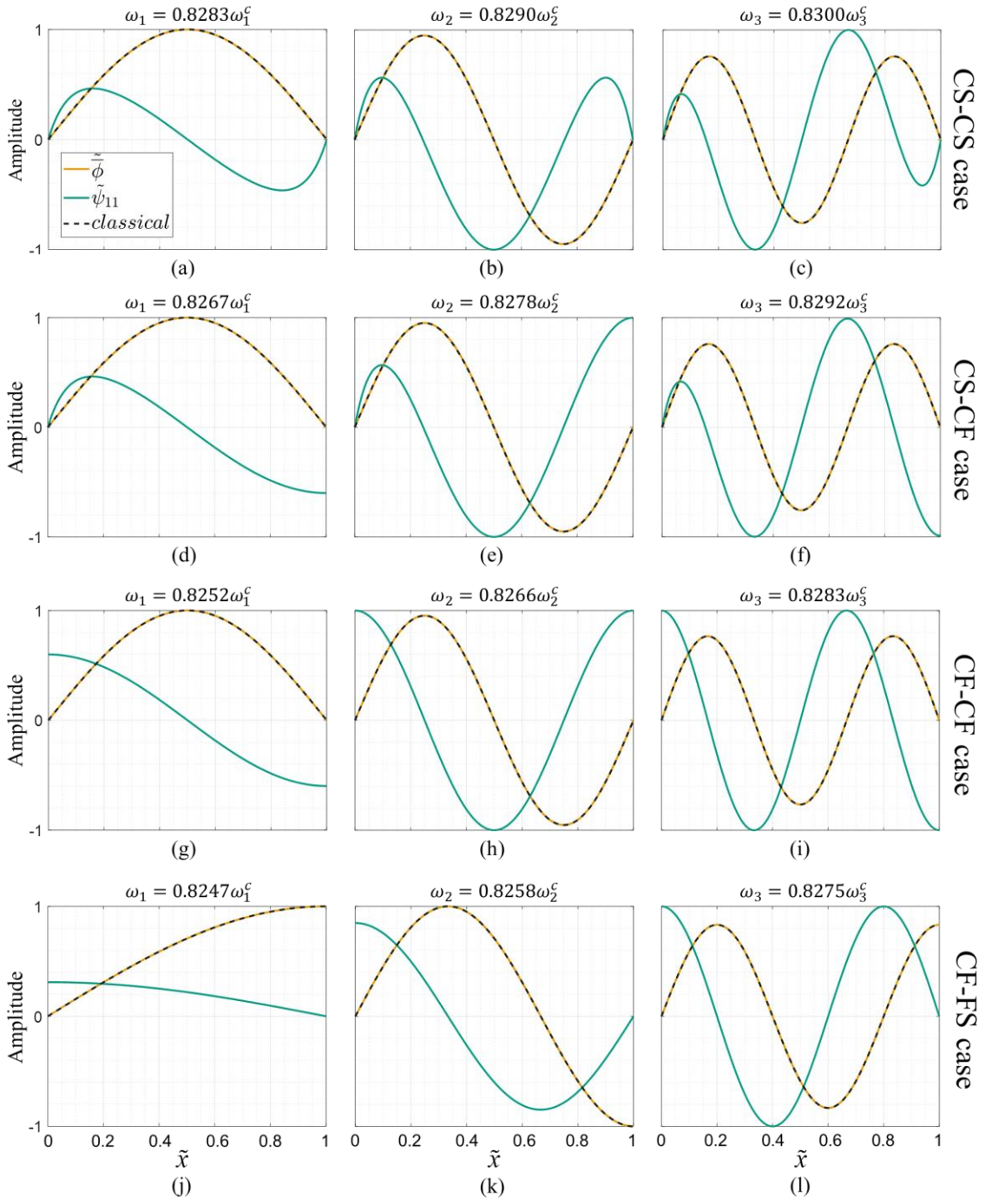

Fig 8. First, second, and third natural frequencies and their corresponding mode shapes for the (a-c) CS-CS case, (d-f) CS-CF case, (g-i) CF-CF case, and (j-l) CF-FS case of boundary conditions for a 1D granular rod with material constants $\alpha_m = 0.5$, $\alpha_{Mm} = -0.4$, $l_s = 0.05$, and $n = 100$.

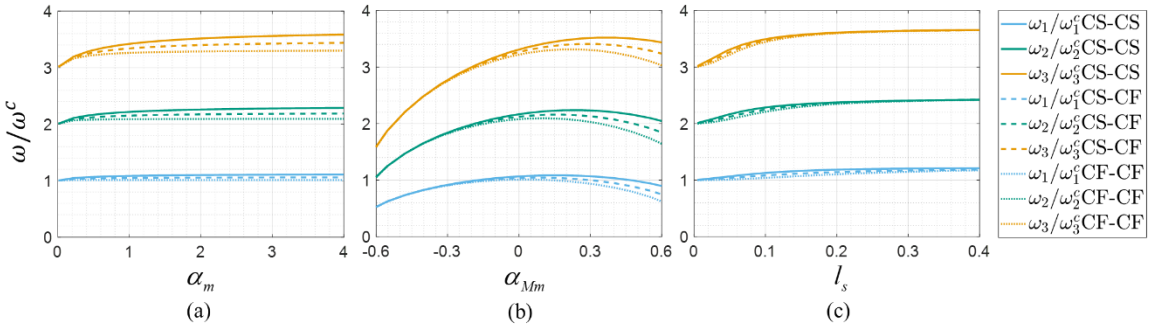

Fig 9. Effect of the material constants (a) α_m, (b) α_{Mm}, and (c) l_s on the first three natural frequencies for a 1D granular rod with material constants based at $\alpha_m = 0.5$, $\alpha_{Mm} = 0$, $l_s = 0.05$, and $n = 100$.